Journal of Applied Physics PERSPECTIVE scitation.org/journal/jap

Characterization methods for defects and devices in silicon carbide

Cite as: J. Appl. Phys. **131**, 140903 (2022); doi: 10.1063/5.0077299
Submitted: 1 November 2021 · Accepted: 23 March 2022 ·
Published Online: 12 April 2022

M. E. Bathen,[1] C. T.-K. Lew,[2] J. Woerle,[1] C. Dorfer,[1] U. Grossner,[1] S. Castelletto,[3] and B. C. Johnson[4,a)]

AFFILIATIONS

[1]Advanced Power Semiconductor Laboratory, ETH Zürich, 8092 Zürich, Switzerland
[2]School of Physics, University of Melbourne, Melbourne, Victoria 3010, Australia
[3]School of Engineering, RMIT University, Melbourne, Victoria 3001, Australia
[4]Centre for Quantum Computation and Communication Technology, School of Engineering, RMIT University, Melbourne, Victoria 3001, Australia

Note: This paper is part of the Special Topic on Defects in Semiconductors.

[a)]**Author to whom correspondence should be addressed:** brett.johnson2@rmit.edu.au

ABSTRACT

Significant progress has been achieved with silicon carbide (SiC) high power electronics and quantum technologies, both drawing upon the unique properties of this material. In this Perspective, we briefly review some of the main defect characterization techniques that have enabled breakthroughs in these fields. We consider how key data have been collected, interpreted, and used to enhance the application of SiC. Although these fields largely rely on separate techniques, they have similar aims for the material quality and we identify ways in which the electronics and quantum technology fields can further interact for mutual benefit.

I. INTRODUCTION

Developments in silicon carbide (SiC) power electronics[1,2] and SiC quantum technologies (QTs)[3–5] are generating significant interest. SiC power metal–oxide–semiconductor field effect transistors (MOSFETs) are finding applications in a broad range of fields from photovoltaic power inverters to electric cars. SiC has quickly become competitive with silicon-based devices in this area, a material closely associated with the electronic age.

Defects in SiC have also made a significant impact on QT with demonstrations of single-photon sources[6,7] and quantum sensing,[8] with a similar application space as the nitrogen-vacancy (NV) center in diamond.[9–11] Commercially available SiC wafers and the well-developed device fabrication protocols make SiC a potentially more viable, cost-effective, and scalable material for QT.

The development of these fields is largely guided by investigations on defect properties, albeit for different aims. Defects in semiconductors arise during crystal growth, fabrication, and even during device operation, especially under the harsh environments that SiC is particularly suited to. All can have a profound impact on device operation but, in the case of QT, defects also present new opportunities. Defects in SiC are an excellent example of this dichotomy: while many defects have a detrimental impact on power electronics, they can also act as single-photon emitters or atomic size qubits showing promise for QT.

Defects that introduce deep energy levels into the semiconductor bandgap can act as charge carrier traps and recombination centers. A prominent example is the carbon vacancy (V_C).[12] The presence of V_C has been correlated with a reduction of minority carrier lifetimes,[13] which in turn is linked to a substantial reduction in device performance. This finding was only made possible through the targeted use and combination of various characterization techniques, including electrical and spin-based measurements.[14]

Where important defects for device technology are marked by their impact on carrier dynamics, quantum centers in semiconductors are often known for binding carriers in stable and isolated localized states. SiC harbors a plethora of defects, which are compatible with quantum computing, communication, and sensing technologies. Key properties include the ability to emit single

photons, long spin coherence times, and coherent spin manipulation. For some applications, the ability to achieve these properties under ambient conditions is also advantageous. Again, the correlation between different characterization methods and theoretical approaches is crucial in identifying defects in SiC that are compatible with QT.

In this Perspective, we aim to highlight the defect–technology relationship and the broad range of defect and device characterization techniques, both traditional and emerging, available for SiC. We further point to the unique ways in which these techniques can be combined to gain an enhanced insight into the properties of defects in SiC. We provide a brief overview of defects in SiC, focusing on their characterization from the perspective of both QT and power electronics. It is our belief that the synergy between these two important application areas can further the success of each. Defects are a common factor in all technologies aiming to utilize SiC due to their perennial presence and strong impact on the electrical and optical properties of SiC materials and devices. Further, we aim to highlight the characterization techniques that we believe are, and will be, important for SiC defect studies in these fields moving forward.

Furthermore, we also note that SiC QT and electronics will both benefit from further innovations in crystal growth and device fabrication techniques. A strong understanding of these areas as well as the related challenges will be as vital to successful defect engineering for QT devices as it is for power electronics. Therefore, only by growing awareness between these fields can greater insight be gained.

We have arranged this work by broadly grouping the techniques into electrical, optical, and magnetic resonance techniques in Secs. III–V, respectively. Other complementary techniques of note are also discussed in Sec. VI. A number of important case studies are discussed in each section and revisited in Sec. VII, which compares the different techniques. Similar successes are expected to greatly advance our knowledge on SiC defects over the coming years and, by doing so, further develop both power electronics and quantum technologies. This will be discussed in Sec. VIII.

II. DEFECTS IN SILICON CARBIDE

SiC is a wide bandgap compound semiconductor with a stoichiometric ratio of Si and C atoms. Each Si atom is covalently bonded to four neighboring C atoms and vice versa. These extremely strong tetrahedral sp^3 hybridized bonds with an energy of 4.6 eV give SiC its impressive structural properties. Depending on the Si-C bilayer stacking sequence, SiC can form different polytypes with slightly differing structural, mechanical, optical, and electrical properties. There is a large number of SiC polytypes to choose from but the most extensively used are the cubic 3C, hexagonal 4H, and hexagonal 6H-SiC polytypes mainly because they are commercially available on the wafer scale.

There is also a broad range of point defects present in SiC but as yet there are just a few comprehensive texts categorizing them in the literature.[15–17] SiC crystal growers have made impressive progress in improving the material quality over the last decade. Large macroscopic defects such as stacking faults, micro-pipes, and carrots have almost been driven to extinction.[18] This has greatly improved the reliability and reproducibility of SiC devices. Indeed, our understanding of fundamental defect properties together with the knowledge on how to integrate them within devices in a controlled manner is rapidly evolving.

Intrinsic SiC defects consist of vacancies (V_{Si} and V_C) and antisites (C_{Si} and Si_C) as well as combinations of these such as the divacancy ($V_{Si}V_C$) and the carbon antisite–vacancy pair ($C_{Si}V_C$). An example of some of these defects is shown in Fig. 1. Additionally, self-interstitials (Si_i and C_i) and interstitial complexes can be formed by various device processing steps. Given the symmetry of the lattice, the same defect can have a range of properties depending on which lattice site it occupies (as indicated in Fig. 1), the Fermi level in the sample, as well as which SiC polytype is used. Although this complicates matters, the lattice site dependence can also be used to elucidate the atomic structure of the defect as discussed further below. Intrinsic defects in SiC can be generated by many methods including laser, gamma, electron, ion, or neutron irradiation to name a few. Defect creation and evolution during device fabrication is another extensive subject that may be

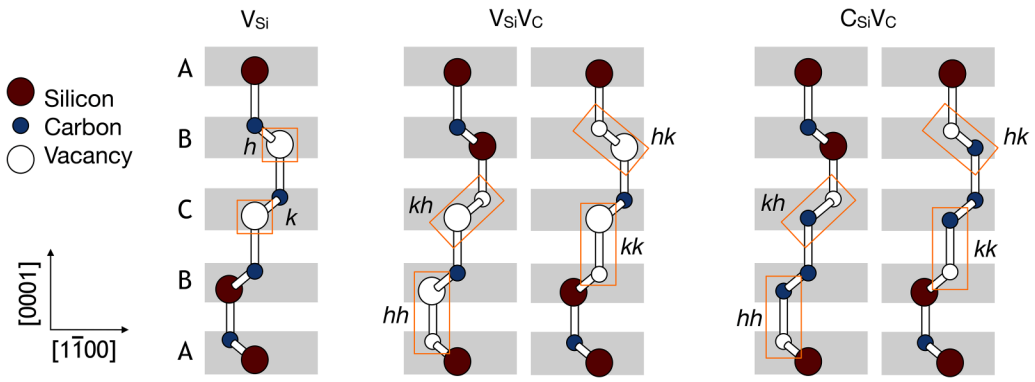

FIG. 1. Schematic of (from left to right) the V_{Si}, $V_{Si}V_C$, and $C_{Si}V_C$ defects in 4H-SiC. The subscripts *h* and *k* refer to the inequivalent hexagonal and quasi-cubic lattice sites, respectively.

addressed another time. However, we note that processes developed for silicon including single ion implantation techniques[19] are also compatible with SiC.

A. Which measurement methods are relevant?

Defect characterization aids the development of methods to eliminate them from active device regions, to harness their properties in new and useful ways, or for their intrinsic interest. Optical and electrical methods of defect characterization have traditionally been utilized to provide insight into the concentration and type of defect present in SiC. Historically speaking, SiC was once used as a lighting material and was the first material in which electroluminescence was systematically studied.[20,21] An early patent filed for a signaling technology, predating telecommunications, is based on this SiC technology.[22] Optical methods of defect characterization were, thus, most relevant for enhancing these properties. Ultimately, other more efficient lighting materials have been developed. Yet, optical emission from defects remains relevant as a quick, highly sensitive method to gauge the presence of defects in SiC without the requirement of device fabrication.

Electrical measurements are of particular relevance for modern SiC devices where defect spectroscopy can be performed even during device operation to gauge their impact. Defect interactions with charge carriers are of fundamental importance for ensuring that device operation is optimal.

More recently, further techniques have been developed to probe the quantum properties of defects. Single defects can now be addressed optically and, in principle, electrically too. The intrinsic spin of these defects can be manipulated both to elucidate the defect symmetry and as a method for quantum information processing. There are a number of recent articles on this subject (see, e.g., Refs. 4, 23, and 10).

B. Defects and technology

SiC is of interest for electronics applications for several reasons. First, SiC inherits some of the outstanding properties of both silicon and diamond. SiC is compatible with many existing industry-standard complementary metal–oxide semiconductor (CMOS) processes and amenable to electrical device fabrication. It is the only wide bandgap semiconductor on which a stable native oxide can be thermally grown. This allows MOSFET devices to be formed in much the same way that silicon devices are.

Like diamond, the wide bandgap and low intrinsic carrier concentration ($n_i = 5 \times 10^{-9}\,\mathrm{cm}^{-3}$ for 4H-SiC at room temperature)[24] of SiC means that it maintains its semiconducting properties at elevated temperatures. A wide range of SiC devices operating at temperatures above 500°C have been demonstrated and are touted to replace existing Si electronics in high-temperature circuits required for various industries (as reviewed in Ref. 1).

Defects impact SiC power electronics in many ways. For example, charge carrier lifetime is an important metric in most electronic devices and defines the extent of conductivity modulation. In SiC, the defect concentration has been clearly linked to reductions in carrier lifetime.[13] V_C are particularly efficient at capturing carriers via Shockley–Read–Hall (SRH) recombination.[25] For devices where carriers flow in the vicinity of the surface, such as when current flow is modulated by an applied gate voltage, defects associated with the SiC bulk–dielectric interface (commonly referred to as the SiC/SiO_2 interface) determine the channel mobility. These defects either act as traps for charge carriers which then screen the applied gate voltage or the trapped charge deflects carriers via Coulomb scattering.

In quantum technology (QT), devices exploit the intriguing properties of localized defect states. Such states appear most commonly for deep level defects in wide bandgap semiconductors. The nitrogen-vacancy (NV) center in diamond is a prominent example.[26] However, the wide bandgap, low spin–orbit coupling, and moderate electron–phonon coupling go a long way in explaining why defects in SiC are emerging as promising contenders for QT applications.

Importantly, QT benefits greatly from developments in material growth capabilities and fabrication protocols, which are mostly driven by the burgeoning SiC electronics industry. As the field continues to develop, we expect this trend to also grow, yielding more sophisticated scalable quantum devices.

Here, we mainly focus on intrinsic point defects but we note that extrinsic impurities are widely used as donors (N, P) or acceptors (Al) to control the conductivity and carrier lifetime of the material, making SiC power devices possible. In QT, extrinsic impurities that introduce deep levels into the bandgap are of interest. These include transition metal impurities (e.g., V, Mo, and Er[27]) and nitrogen dopants, which makeup the $N_C V_{Si}$ defect in SiC (the SiC counterpart of the NV center in diamond).[28] These are particularly important as they exhibit optical emission in the telecom range and are, therefore, highly compatible with current fiber optic infrastructure for quantum communication technologies. An overview of the unambiguously identified electrically active defects originating from extrinsic impurities is presented in Ref. 17.

We now turn to defect characterization in SiC using electrical, optical, magnetic, and other complementary techniques.

III. ELECTRICAL TECHNIQUES

Electrically active defects have a profound impact on SiC electrical device operation as they can severely limit the mobility in MOSFET devices via carrier trapping and scattering processes.[29] The electrical techniques mentioned in this section have been pivotal in developing fabrication processes to reduce the detrimental effect of defects, optimize device function, and increase our understanding of their formation and behavior.

Figure 2(a) illustrates the broad range of electrical-based characterization techniques available and the regions in the bandgap that they are generally able to probe. Hall and capacitance–voltage (CV) measurements are most sensitive to shallow levels from which electron or hole carriers can be thermally excited. Thermal admittance spectroscopy (TAS) has most often been used to measure the thermal activation energies (using an Arrhenius-type analysis) and densities of shallow impurities.[30] Deep level transient spectroscopy (DLTS), a complementary technique to TAS,[31] is best suited to the characterization of deep levels, which often act as efficient recombination centers. For QT, these deep levels are of prime interest since they are largely isolated from their environment, reducing thermal perturbations that may degrade spin properties. Minority carrier

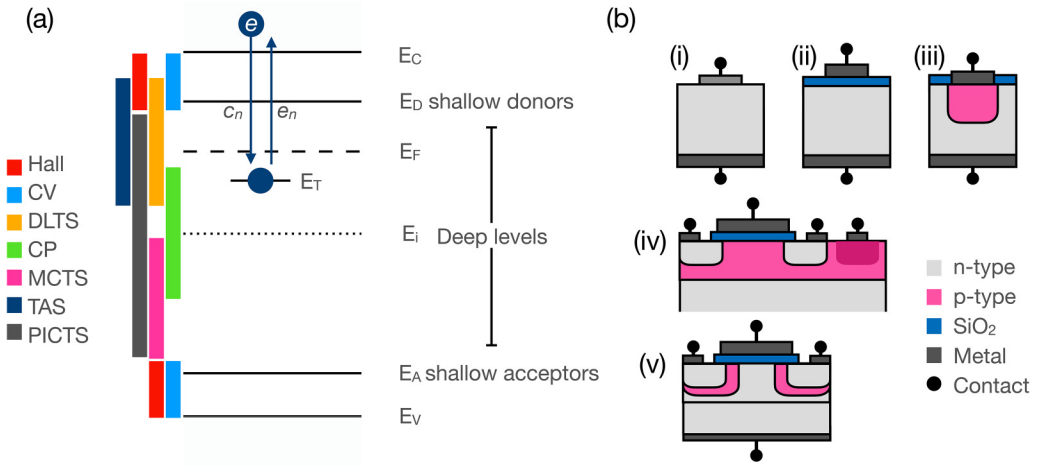

FIG. 2. (a) Schematic of the energy range over which various electronic characterization techniques are sensitive for an n-type semiconductor, including capacitance voltage (CV), deep level transient spectroscopy (DLTS), charge pumping (CP), minority carrier transient spectroscopy (MCTS), thermal admittance spectroscopy (TAS), and photo-induced current transient spectroscopy (PICTS). (b) Schematics of cross sections of common device geometries used for these measurements including (i) Schottky contact, (ii) metal–oxide–semiconductor (MOS) capacitor, (iii) pn junction diode, (iv) a lateral p-channel depletion mode MOSFET, and (v) a power MOSFET.

transient spectroscopy (MCTS) also probes deep level traps but for the opposite carrier type.[32,33] Photo-induced current transient spectroscopy (PICTS) is based on the same principles of carrier emission from traps as DLTS but the filling pulse is provided by light excitation (often above bandgap energies and requiring the use of transparent electrical contacts) while a reverse bias is applied to the device. The time constants associated with a series of current transients are then recorded as a function of temperature.[34] The fingerprint defect energy level and optical capture cross section are then determined via an Arrhenius analysis similar to DLTS or TAS.

Electrical defect characterization typically requires the fabrication of a device. Figure 2(b) displays the schematics of common device geometries used for these measurements including, in order of fabrication complexity, (i) a Schottky contact, (ii) a metal–oxide–semiconductor (MOS) capacitor, (iii) a pn junction diode, (iv) a p channel depletion mode MOSFET, and (v) a power MOSFET. In this section, we illustrate the versatility of electrical techniques through examining two key case studies: SiC/SiO_2 interface related defects and the V_C defect. These two defect types, in particular, have been extremely important in improving SiC electrical device operation.

A. Capacitance–voltage

Capacitance-based measurements are an extremely popular way to characterize defects in SiC devices due to their efficiency, availability, and relatively high sensitivity. The required setup is straightforward: a DC voltage superimposed with an AC probe voltage with a small amplitude—usually around 30 mV (the thermal energy at room temperature, k_BT)—is applied across a device. Simple devices are sufficient to perform this experiment successfully as long as the leakage current is minimal. Schottky barrier diodes are a well-developed technology in SiC and common Schottky metals are reviewed in Ref. 35. Pn junctions are also appropriate and have the advantage that a ready source of minority carriers is available to respond to the AC probe. MOS test capacitors are also possible especially for characterizing defects at the SiC/SiO_2 interface.[36]

A broad range of capacitance-based techniques are available to probe deep levels in the bulk and at the SiC/SiO_2 interface. Many of these techniques were developed for Si characterization but may be applied to SiC with careful interpretation. For SiC/SiO_2-interface characterization, these include the Terman (C/ψ_s),[37,38] Hill-Coleman (single frequency CV/GV),[39] quasi-static,[40] high-low,[41] and conductance[42,43] methods.

Following the nomenclature employed for silicon, we categorize the various SiC/SiO_2-related defects as interface charge, fixed oxide charge, mobile ionic charge, and oxide charge. The two most relevant for our discussion are interface and fixed oxide charge. Interface trapped charge is often associated with a dangling bond at the interface. These are expected to contribute a broad band of states around midgap. Fixed oxide charge is generally associated with the E' center (trivalent Si defects in the oxide). These lie within the oxide and do not electrically exchange charge with the underlying SiC substrate. In addition to these defects, there is another distinct category referred to as near interface oxide traps (NIOTs) that *do* electrically communicate with the substrate.

Each of these defects has a distinct impact on a standard CV curve. Figure 3 shows CV traces for a n-type SiC/SiO_2 device before and after a 60 min post-oxidation anneal (POA) in nitric oxide (NO).[44] Fixed oxide (positive) charge causes a voltage shift of the CV curve toward negative voltages. Interface states cause a stretch-out along the voltage axis which can be seen on comparison to the simulated CV curve plotted in Fig. 3 which assumes no defects. This arises since these defects become charged as band

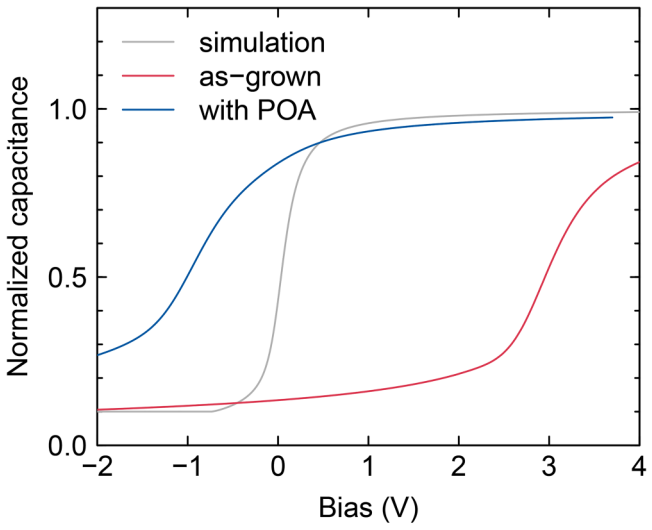

FIG. 3. CV of 4H-SiC MOS capacitor before (red curve) and after (blue curve) a post-oxidation anneal in NO. The gray curve represents a simulation without defects at the interface.

bending at the surface sweeps the Fermi level through the density of states, thereby contributing a varying offset voltage.

The voltage sweep rate and direction can be varied to probe NIOT type defects. NIOTs with a slow time constant may cause a hysteresis of the CV as the voltage is swept from inversion to accumulation and back again. Fast NIOTs may cause the extent of stretch-out to change depending on which direction the voltage is ramped. The response of NIOTs to an AC probe voltage involves both a tunneling mechanism and carrier capture/emission processes. Therefore, care must be taken when quantifying trap properties using this basic technique.[36] This measurement allows the concentration of these defects to be quantified via the amount of charge that they produce and also their energy distribution through the bandgap.

The NIOTs have been paid particular attention in SiC/SiO_2 devices since they appear to be much more prominent than dangling bonds and are thought to be responsible for the voltage shift instability phenomena.[16,44–47] However, the defect identification that may allow more efficient methods to control their densities remains elusive. Tentative proposals for NIOTs include oxygen deficiencies[48,49] or silicon interstitials[50] or even silicon vacancy related defects on the bulk SiC side of the interface.[51,52] The role of carbon in these defects is controversial. The carbon cluster picture of the SiC/SiO_2 interface is indeed convenient. Further, it is generally accepted that high concentrations of carbon exist at the SiC/SiO_2 interface.[53,54] Yet, direct and unambiguous experimental evidence for the atomic form of NIOTs remains lacking. Their identification and quantification remains an active area of research especially with the aim of reducing their density through various passivation techniques such as NO POA to enhance the channel mobility of SiC transistors. We expect their reduction in devices for QT applications will also be beneficial. Spin qubit defects that may be close to the surface so that they can be finely controlled with surface gates are generally sensitive to magnetic and charge noise. A high-quality SiC/SiO_2 interface would, therefore, improve the spin coherence properties and stability.

Interestingly, according to theoretical calculations, energy levels can also be formed close to the band edges based on how the unit cell is terminated at the surface.[55] This local modification of the bandgap may also have an impact on other defects that reside close to the interface.

B. Deep level transient spectroscopy

Deep level transient spectroscopy (DLTS) is a powerful defect spectroscopy technique used to detect low concentrations of point defects—typically around four orders of magnitude less than the carrier concentration. The technique has been extensively used to understand the types and quantities of electrically active defects in SiC especially in the bulk rather than at the SiC/SiO_2 interface. Developing an understanding of bulk defects is vital for realizing the full potential of SiC devices, but understanding the complete energetics of defects is also becoming more important in the QT context, as charge state control, electrical driving, and device integration become more important.

Standard DLTS makes use of the ability to sweep majority carriers in and out of the region close to a pn-, Schottky junction or MOS interface by applying forward and reverse biases across the device. Within the depletion region, majority carrier traps are at equilibrium and not occupied. These traps can be filled by application of a short voltage pulse across the device forcing majority carriers to sweep into this region. The pulse duration is long enough to ensure full trap occupancy. Once the majority carriers are swept out of the probed region, majority carrier emission from defects occurs. During this process, the depletion region will contract to its equilibrium value. This can be measured by monitoring the change in capacitance, current, conductance, or charge transient across the device. Depth profiling of the defect concentration profile can also be achieved by stepping the voltage amplitude of the trap filling pulse through the depletion region. By combining DLTS and MCTS measurements for the same device, defects with energy levels in both the upper and lower portions of the bandgap can be observed.

Simple device structures similar to those used for CV measurements are sufficient for DLTS. Pn junctions have the added advantage that minority carriers are readily available and can also be swept into the probed region.

The position of the Fermi level determines which levels in the bandgap become filled during the filling pulse. Spectroscopy of the traps is usually achieved by changing the temperature of the device, which shifts the Fermi level position. Generally, for wide bandgap semiconductors, only the upper one-third of the bandgap can be accessed. High temperatures are used to push the Fermi level toward midgap but in doing so, some defects can be annealed out. This can be observed in high-temperature DLTS studies where the spectrum is scanned multiple times.[56] At lower temperatures where the Fermi level moves toward the band edges, carrier freeze-out can occur due to incomplete ionization. For moderately Al-doped p-type 4H-SiC with an acceptor level situated ~0.2 eV above the

valence band, carrier-freeze-out occurs typically around 150 K. Below these temperatures, trap filling may be incomplete and an increase in series resistance may attenuate the measured capacitance.

The most prominent defect probed with DLTS in bulk n-type 4H-SiC is the $Z_{1/2}$ defect which is a negative-U center, more stable when capturing two electrons.[57] It is often found in as-grown material in the 10^{12}–10^{13} cm^{-3} density range[58] and can severely limit the bulk minority carrier lifetime.[59] The $Z_{1/2}$ signal is considered to be associated with the V_C occupying inequivalent h and k lattice sites.[14] Identification of this important deep level defect was made possible through the correlation of electrical measurements, theoretical calculations, and magnetic resonance techniques (we will return to this topic below). Further support for this assignment was presented in a series of works by two separate groups on SiC oxidation that injects interstitial carbon atoms into the substrate.[59–62] The $Z_{1/2}$ signal was found to be directly modified by this process with the decrease in the total $Z_{1/2}$ concentration proportional to the oxide thickness. Remarkably, the $Z_{1/2}$ concentration could be reduced to below the detection limits of the DLTS technique, i.e., $<10^{11}$ cm^{-3}. The carrier lifetime was found to be significantly enhanced by the process.[13,62]

An example DLTS spectrum of the $E_{1/2}$ defect (the 6H-SiC equivalent of the $Z_{1/2}$ defect in 4H-SiC)[63] is shown in Fig. 4(a) obtained from a p^+n junction device. The convoluted signal situated around 160 K can be resolved by fitting two Gaussian functions. From the temperature at which each Gaussian is situated, the trap energy level and capture cross section can be determined using the Arrhenius relation for different rate windows (related to the trap emission rate), as shown in Fig. 4(b). The trap concentration is related to the amplitude of the signal, which is equal to 4.8×10^{14} cm^{-3} and 3.9×10^{14} cm^{-3} for the E1 and E2 defects, respectively, in this case. Compared to 4H-SiC, there exist three inequivalent lattice sites (h, k_1, and k_2) in 6H-SiC. High energy resolution Laplace-DLTS is required to fully resolve the carbon vacancy at all three non-equivalent lattice sites.[64]

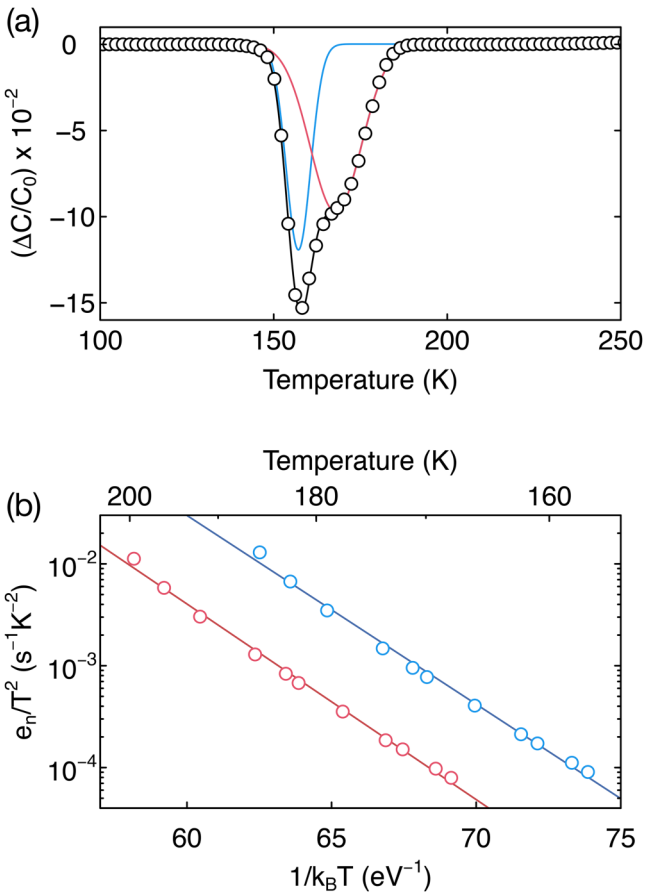

FIG. 4. DLTS analysis of a 6H-SiC p^+n junction diode showing (a) the DLTS spectrum of the E1 (blue curve) and E2 (red curve) defects using a rate window of 420 ms and (b) the Arrhenius analysis of these peaks giving energies $(E_C - E_T) = 0.427 \pm 0.010$ eV and $(E_C - E_T) = 0.442 \pm 0.009$ eV, respectively.

C. Charge pumping

Charge pumping (CP) is an alternative highly sensitive defect spectroscopy technique widely used to quantify the mean interface state density, $\overline{D_{it}}$, in the vicinity of the SiC/SiO_2 interface. The $\overline{D_{it}}$ here is expected to contain contributions from NIOT type defects in addition to interface defects. However, CP is generally not sensitive to traps with long emission times. In contrast to CV methods, CP is performed with a fully fabricated MOSFET device. After undergoing full fabrication, which may include dopant implantation or diffusion and high-temperature thermal processes, the types and quantities of defects can change dramatically. Although test capacitors for CV measurements can be incorporated on-chip, CP measurements are most relevant for probing the impact of these processes. The technique has most extensively been applied to Si MOSFETs but has also found success with their SiC counterparts.[65] Both standard four-terminal lateral MOSFETs and three-terminal MOSFETs that typically employ vertically diffused MOSFET (VDMOSFET) device structures are compatible with the technique.[66,67]

The experimental setup is relatively simple and cost-effective (function generator and ammeter) and the rapid measurement capability of the CP technique makes it an ideal quality control tool in a semiconductor production line to evaluate the MOSFET interface quality. Figure 5(a) shows a schematic of a n-channel SiC MOSFET setup for a CP measurement. A trapezoidal voltage pulse is applied to the gate contact, pumping the device between accumulation and inversion, while the source and drain contacts are tied together and shorted to ground. The resulting CP current, I_{CP}, measured from the bottom contact due to recombination of majority and minority charge carriers at the SiC/SiO_2 interface is directly proportional to the mean interface state density.[68] Figure 5(b) shows standard data for a SiC MOSFET. Only fast interface traps can contribute to the CP current where trap emission can proceed within the pulse time. In fact, this attribute can be leveraged to address defects with specific time constants such as slow traps or even NIOTs.[69]

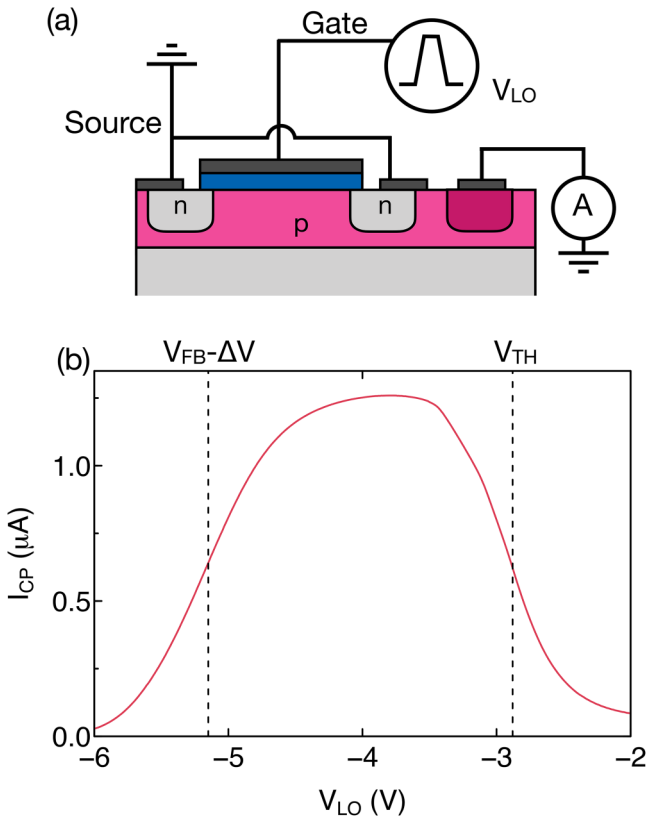

FIG. 5. (a) Schematic of a SiC MOSFET setup for CP measurements. (b) Charge pumping current as a function of the base voltage, V_{lo}, for $\Delta V = V_{hi} - V_{lo} = 4$ V. The CP current curve is bounded by $V_{FB} - \Delta V$ (the flatband voltage minus the energy window accessed by the voltage pulse) and the threshold voltage V_{TH} of the MOSFET.

The maximum CP current is directly proportional to the interface state density, which in this case is approximately 1.9×10^{11} cm^{-2} eV^{-1}. From the line shape of the CP curve, estimates of the flatband and threshold voltages can also be extracted.[70] As with CV curves, this may give a relative measure of fixed oxide charge density if the CP curve is observed to shift along the x-axis. Further variations of CP have been developed to give the spatial and energy distribution of traps.[71–73] However, CP is not particularly sensitive to defects with energy levels close to the band edges.

In terms of the sensitivity, CP can measure defect densities down to 10^{11} cm^{-2} eV^{-1}. However, for devices with reduced dimensions and fast CP pulses in the MHz regime, it may also be possible to address individual interface traps as demonstrated with silicon MOSFETs.[74] Addressing a single spin for possible QT applications has not yet been demonstrated using this method but may yield a promising spin readout protocol. In this context, the CP technique may also be integrated with magnetic resonance methods. This combination significantly enhances the spectroscopic power of the technique and is discussed further in Sec. V A.

In summary, a broad range of electrical techniques that have mostly been developed for silicon devices can be applied to SiC. Two example case studies were discussed: characterization of defects at and near the SiC/SiO$_2$ interface and identification of the $Z_{1/2}$ deep level trap as the V_C. Of course, care must be taken in the interpretation of results mostly because of the complicating presence of carbon. Furthermore, the NIOT defects appear to play a more significant role in the electrical characteristics of SiC electronic devices than for Si. Recent QT focused works are starting to draw upon SiC electronics technologies, made possible by these defect characterization techniques. Defect spins can now be addressed and coherently controlled, which may develop into a broadened application space for SiC. In Sec. IV, we will outline how optical techniques have had a distinct role in the development of SiC technologies but one that also points to similar developments.

IV. OPTICAL TECHNIQUES

A. Photoluminescence

Photoluminescence (PL) spectroscopy is a central technique for the characterization of defects in SiC, with the capability of detecting low defect densities across the entire device volume from surface to substrate. It involves the excitation of electronic states and the detection of spontaneous emission as these states de-excite. Figure 6(a) shows a schematic of the wavelength regions where emission is detected in 4H-SiC for both band-to-band

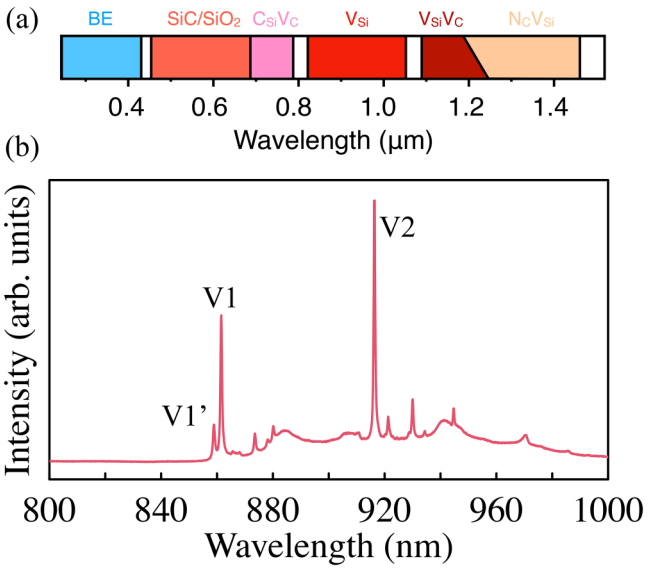

FIG. 6. (a) The broad wavelength range over which various PL signals can be found in 4H-SiC. These include band-edge (BE) related PL, and PL from SiC/SiO$_2$-related defects,[44] $C_{Si}V_C$,[75] V_{Si},[76] $V_{Si}V_C$,[77] and N_CV_{Si}.[78] The ZPL wavelengths will be summarized in Table I. (b) An example PL spectrum of V_{Si} in proton-irradiated 4H-SiC measured at 80 K. The V1 and V2 ZPLs arise from the $V_{Si}(h)$ and $V_{Si}(k)$ defects, respectively. V1' is a higher lying excited state of $V_{Si}(h)$. The 532 nm laser excitation employed to obtain this spectrum was directed perpendicular to the c-axis to enhance the ZPL intensity.

recombination (below 400 nm) and SRH recombination at defect states. As shown, SiC defect-related PL covers an extremely broad spectral range from the UV to the NIR.

The equipment for PL consists of a light source for excitation, focusing optics, a sample stage that may include temperature and motion control for PL mapping and a spectrometer. There are many commercial systems available but home-built systems are also common that allow the experiment to be integrated with other capabilities. No special device requirements are needed, only that the excitation laser interacts with the sample (i.e., no opaque metals or packaging layers).

The V1/V2 spectrum associated with the V_{Si}^{-} defect in 4H-SiC is shown in Fig. 6(b). Like many defect related spectra, this consists of two parts. The high energy side of the spectrum has a zero phonon line (ZPL), which arises from direct electronic transitions [labeled V1 and V2 in Fig. 6(b)]. ZPLs are readily observable at low temperature in SiC (<150 K) and are often used to identify the type of defects present.[75,79–81] Some commonly observed and defect related ZPL wavelengths in 4H-SiC are summarized in Table I.

The second component of a PL spectrum is the much broader phonon (or vibronic) sideband (PSB), which arises from electron–phonon coupling and appears on the low energy side of the ZPL. These can sometimes be used to further elucidate the defect identity especially via theoretical methods.[82]

Polarization studies of the ZPL can reveal the symmetry and transition dipoles of the defect.[90] There are many PL signatures in SiC that have been reported but have not yet been assigned to a particular atomic defect.[80,81] Understanding the origins of these defects, their role in devices and their possible use in applications remains an extremely active and interesting area of research.

TABLE I. Prominent defects in 4H-SiC and their associated spin values and zero phonon line (ZPL) wavelengths. ZPL wavelengths are approximate given they are determined at a range of different temperatures. Note that in different polytypes the bandgap changes and so do the defect's emission wavelengths.

Defect	Spin	ZPL (nm)	Label	References
$(C_{Si}V_C)^{+}$	S = 1/2	648.6	A1	6 and 75
		651.8	A2	
		665.1	A3	
		668.5	A4	
		671.7	B1	
		673.0	B2	
		675.2	B3	
		676.5	B4	
V_{Si}^{-}	S = 3/2	861.5	V1	76
		916.3	V2	
$(V_{Si}V_C)^{0}$	S = 1	1128.2	PL1	77, 83, and 84
		1127.1	PL2	
		1106.0	PL3	
		1076.3	PL4	
$(N_CV_{Si})^{-}$	S = 1	1179.7	PLX4	78, 28, and 85
		1222.7	PLX3	
		1241.0	PLX2	
		1242.3	PLX1	
V^{4+}	S = 1/2	1278.8	α	86
		1335.3	β	
Cr^{4+}	S = 1	1042	Cr_C	87 and 88
		1070.3	Cr_A	
Mo^{5+}	S = 1/2	1076		89

There is a ZPL for each inequivalent site in the lattice since each site has a slightly different local environment.[76,91] An important example for optical characterization of defects in SiC is the negatively charged V_{Si}^{-} defect, which takes up one lattice site, has two ZPLs in 4H-SiC [V1(h) = 862 nm and V2(k) = 917 nm as shown in Fig. 6(b)], three in 6H-SiC [V1(h) = 865 nm, V2(k_2) = 887 nm and V3(k_1) = 908 nm],[92] and one in 3C-SiC (at 645 nm).[93] The peak labeled V1' in Fig. 6(b) arises from a higher lying excited state of $V_{Si}^{-}(h)$. The Si vacancy is important for QT applications and was identified (down to lattice site dependency) by combining PL spectroscopy, magnetic resonance techniques and theoretical calculations.[76]

Another particularly interesting defect with a strong optical signature is related to the SiC/SiO_2 interface.[94–96] The atomic origin of the defect has not yet been identified; however, its PL signature contains features that may be associated with the vibrational modes of oxygen and carbon bonds. The defect density is also approximately 10 times greater on the C-face than on the Si-face further supporting the possible role of carbon.[44] This class of defect possesses a variable ZPL that appears within the wavelength range 450–700 nm independent of the SiC polytype considered.

The emission and absorption dipoles of these SiC/SiO_2-related defects are both aligned with the basal plane bonding direction of the underlying SiC crystal. There is some variability in this alignment, suggesting that they may exist in a slightly disordered environment, i.e., perhaps within the transitional layer between the oxide and SiC substrate. The defects can also be driven electrically meaning that at least some are in electrical communication with the substrate and may have an impact on carrier trapping.[95] Interestingly, the intensity of these emitters is also sensitive to electric fields.[97]

The polarization visibility of the SiC/SiO_2 interface-related defects is high (i.e., emitted photons are predominantly polarized) meaning that quantum protocols that require polarized photons to encode information can retain high count rates (typically >300 k counts per second or several times brighter than the NV center in diamond) without loss through additional polarization optics. These defects do not appear to exhibit properties that would indicate the presence of spin suggesting transitions between singlet states.

Finally, the SiC/SiO_2-related defects have been shown to have a defect density that correlates well with electrical measurements on the SiC/SiO_2 interface states, including DLTS[98] and CV.[44] This suggests that PL measurements could be a powerful production line tool to assess the quality of the SiC/SiO_2 interface at any stage of device fabrication. Wafer-scale band-edge PL mapping systems are already commercially available. On this note, PL mapping of charge sensitive defects such as the V_{Si} defect may also be mapped during device operation to image regions of trapped charge as demonstrated with the NV center in diamond.[99]

In terms of QT, there are a number of key metrics that can be determined with PL spectroscopy,[5] an example being the ZPL linewidth and the Debye-Waller factor which is the ratio between the

integrated ZPL intensity to the total spectrum (ZPL:PSB). A defect that predominantly emits light into one spectral mode will have greater utility. These metrics can be enhanced by the integration of these defects into SiC photonic cavity devices.[100] These devices enhance the emission count rates and spectral purity and channel the emission into single mode fibers or waveguides with high collection efficiency. This is often an obstacle in materials such as SiC and diamond due to the high refractive index and dipole emission of these defects.[90] For example, the V_{Si} defect has a single dipole along the c-axis so that emission is preferentially directed perpendicular to the c-axis (usually along the surface direction). This may make planar photonic structures such as on-chip waveguides more attractive in this case, which is yet to be fully explored.

B. Single-photon detection

Quantum technology devices engineered from semiconductor defects rely on single defect control. Controlling defect qubits requires single-spin readout while quantum communication devices are based on the emission of a single photon with a controlled rate. Ensemble methods as outlined above are not suitable for these application areas, necessitating tuning of the PL setup toward the single defect regime.

Figure 7(a) shows a typical confocal setup for single defect spectroscopy, which consists of a dichroic mirror to direct the laser light down through an objective lens to the sample. The PL light is collected back through the lens. Any reflected laser light is removed with the dichroic mirror and long pass filter. After the filter, a confocal pinhole will collect light from a small excitation volume within the sample. For example, for a 532 nm laser directed through a 0.95 numerical aperture (NA) objective, the lateral resolution is $0.4\lambda/NA = 224$ nm and $1.4\lambda\eta/(NA)^2 = 2.2\,\mu$m in the axial direction for a SiC refractive index of $\eta = 2.66$. Longer excitation wavelengths may be employed to better overlap with the absorption band of the defect of interest.

This system can be integrated with a scanning stage to allow 2D mapping of the sample as shown in Fig. 7(b) of a SiC sample after an oxidation at 1000 °C resulting in a 14 nm surface oxide. This results in the formation of SiC/SiO_2 interface related defects, which appear as bright diffraction limited spots in this image.

The emitted light from the defect can be directed to an avalanche photodetector (APD), photomultilier tube, or superconducting nanowire single-photon detector for sensitive PL mapping. In the case of Fig. 7(a), a beam splitter and a pair of APD single-photon counting modules can be used as the basis of a Hanbury Brown Twiss interferometer. This interferometer quantifies the single-photon emission purity of the emitter through an autocorrelation measurement, $g^{(2)}(\tau)$.[101] This is essentially a histogram of delay times between detection events on the two detectors. An example is shown in Fig. 7(c) for the defect indicated by the box in Fig. 7(b). From the shape of this trace, we deduce that the defect is a single-photon emitter and that its excited state lifetime is 3 ns. The bunched shape for $g^{(2)} > 1$ suggests that recombination involves a three-level system. In terms of single defect spectroscopy, we can then perform measurements on the properties of single defects that would usually be obscured in an ensemble measurement.

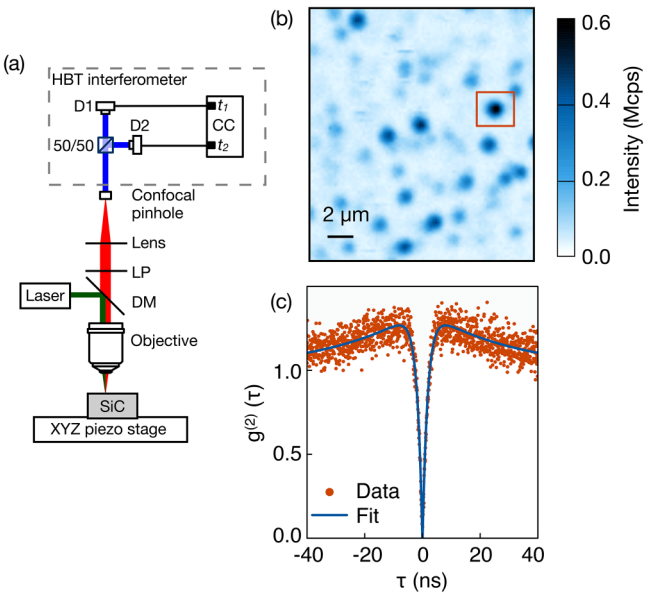

FIG. 7. (a) Schematic of a typical confocal microscopy setup consisting of a laser source, dichroic mirror (DM), and long pass (LP) filter to direct only the PL into the confocal pinhole through to the two APD detectors (D1 and D2) of the Hanbury Brown Twiss (HBT) interferometer. A correlator card can record the time between events on the two detectors. (b) A confocal map of the SiC/SiO_2-related defects. Each spot is a single defect. Single-photon emission of the defect indicated by the orange box is confirmed by the autocorrelation function $g^{(2)}$ measurement in (c). This shows a histogram of the delay times measured between events detected on the two APDs. For a SPE, photons at $\tau = 0$ s should be zero. Two photon sources would at best give $g^{(2)} = 0.5$ so a SPE is usually defined as $g^{(2)} < 0.5$.

This has allowed the PL spectrum of single SiC/SiO_2-related defects to be obtained bringing us a step closer to defect identification.

In QT, SPEs are a key component of quantum networks used to carry quantum information. As mentioned above, photonic cavity structures fashioned into the SiC surface can enhance the outcoupling efficiency of the emission. This is particularly important for single defects like V_{Si} and $V_{Si}V_C$, both of which have inherently low single-photon emission count rates (10–20 k counts per second). The enhancement can, therefore, reduce measurement noise and collection times.

Various QT protocols require indistinguishable photons for entanglement. In this case, the single photon emission should have a ZPL that is Fourier transform limited. The indistinguishability is assessed in a Hong-Ou-Mandel interference experiment where the probability of photon pairs exiting a beam splitter through the same arm is measured.[102] Indistinguishable photon emission from the V_{Si} defect has successfully been demonstrated to a contrast close to 90%.[103] It is sometimes also preferable to have emission in the telecom wavelength range to avoid losses in standard optical fiber infrastructure. Defects like the $N_C V_{Si}$[85] and vanadium impurities[86] are of particular interest for this reason with their telecom wavelength emission.

V. MAGNETIC RESONANCE TECHNIQUES

In this section, we discuss how the electrical and optical techniques discussed above can be enhanced by combining them with electron spin resonance (ESR) techniques. ESR is a measurement technique sensitive to paramagnetic defects having unpaired electrons. In an applied magnetic field, the spin sublevels will split that allows spin flips (transitions between these sub-levels) to be induced via absorption of electromagnetic irradiation, usually at microwave (MW) or radio frequencies.

ESR has played a pivotal role in identifying several important defects in SiC, including the V_C,[104] $V_{Si}V_C$,[105] $C_{Si}V_C$,[106] and the V_{Si} defect.[107] The main drawback of the ESR technique is its sensitivity. This is mostly due to defect spin sub-level populations being governed by the Boltzmann distribution. As a consequence, commercial X-band (~9.7 GHz) ESR spectrometers are only sensitive to around 10^{11} spins/mT linewidth at room temperature.[108]

To overcome this issue, alternative detection approaches have been developed in which spin-dependent charge transport processes or spin-dependent optical transitions are monitored instead. The techniques that utilize these alternative spin-dependent processes are electrically detected magnetic resonance (EDMR) and optically detected magnetic resonance (ODMR), respectively. Both techniques are able to study a small ensemble of spins several orders of magnitude less than the ESR spin sensitivity limit.

A. Electrically detected magnetic resonance

Several charge transport processes have been found to be affected by the spin state of paramagnetic defects. These include spin-dependent recombination, hopping, and tunneling. All mechanisms involve two interacting spins obeying spin selection rules such that the symmetry of the spin-pair directly influences the charge transport process. This can be detected as a change in the device conductivity.

A schematic of the spin-dependent recombination (SDR) process is shown in Fig. 8(a) for n-type SiC.[109] Prior to the completion of the SDR recombination process, a paramagnetic defect (with an energy level at E_T) and a conduction band electron form a temporary effective $S = 1$ intermediate spin-pair. As the recombination process requires the total spin angular momentum of the system to be conserved, assuming negligible spin–orbit coupling, only the spin-pair in a singlet state is able to complete the recombination process subject to coherent ESR excitation, whereas the spin-pair in one of the three possible triplet states dissociates.

The main components of an EDMR spectrometer are shown in Fig. 8(b) and include a homogeneous magnetic field controlled with a programmable power supply and a MW signal generator. The MW signal is delivered to the device via a MW antenna to induce spin transitions. The device can be a pn junction or a MOSFET type device. The biasing conditions of the device must be tuned to optimize the spin-dependent component of the measured current via a transimpedance pre-amplifier. The current signal can be quite small so a lock-in amplifier can be beneficial. The current is then measured as a function of the applied magnetic field. The EDMR signal from a 6H-SiC n^+p junction diode collected at room temperature is shown in Fig. 8(c). This particular defect is not yet identified but it has a Landé g-factor of $\mathbf{g} = 2.0137$ determined from the resonance condition, $\Delta E = hf_{MW} = \mathbf{g}\mu_B B$, where μ_B is the Bohr magneton, h is the Planck constant, $f_{MW} = 8.31$ GHz and, $B = 294.8$ mT directed along the c-axis of the SiC device. A set of hyperfine features separated by approximately 1.23 mT is also observed, corresponding to a hyperfine coupling constant of 34.6 MHz.

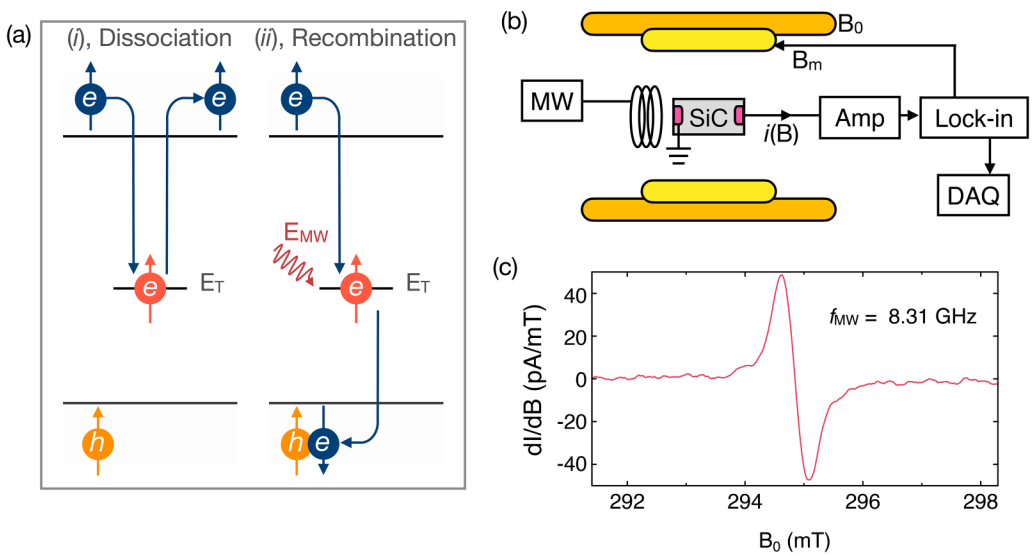

FIG. 8. (a) Illustration of the spin-dependent recombination process in which an intermediate spin-pair in the triplet state ($S = 1$) dissociates, whereas the triplet spin-pair can become a singlet state ($S = 0$) subject to coherent ESR excitation such that the recombination process can be completed. (b) Simplified schematic of an EDMR spectrometer. (c) Typical EDMR spectrum from a 6H-SiC n^+p junction diode. The signal originates from an unidentified processing-induced defect.

Additional measurements may involve measuring these parameters as a function of magnetic field direction to map out the full **g** tensor and hyperfine coupling tensor. This will allow the defect symmetry to be identified. Additionally, ESR techniques involving different MW pulse sequences may be applied to the sample to characterize the spin–spin and spin–lattice relaxation times. These are important metrics for QT operations.

The data displayed in Fig. 8(c) were obtained under a constant DC bias. For a MOSFET device structure, several biasing schemes have been developed to address paramagnetic defects at the oxide interface in an EDMR measurement, including the gate-diode,[110] bipolar amplification effect (BAE),[111] and CP biasing configuration[112] (Sec. III C). Both the gate-diode and BAE biasing configuration utilize a constant DC bias, whereas the CP biasing configuration applies an AC bias to the gate contact. The gate-diode biasing configuration has a sensitivity of $\Delta I/I_0 \sim 1.4 \times 10^{-5}$, while the BAE biasing configuration offers the highest sensitivity reported to date ($\Delta I/I_0 \sim 6.8 \times 10^{-2}$).[111] These DC biasing methods are only sensitive to interface defects residing near midgap. The dynamic nature of the CP biasing configuration allows a large proportion of the SiC bandgap to be probed at room temperature, although it is not as sensitive as BAE ($\Delta I/I_0 \sim 8.2 \times 10^{-3}$).[113] Furthermore, CP-EDMR is only sensitive to defects and spin processes that are able to respond to the CP frequency (usually >100 kHz). Complementary EDMR measurements can be performed with both the BAE and CP biasing configurations, which in some instances can address and reveal different interface defect signatures.

Identifying the atomic structure of the SiC/SiO_2 interface defects responsible for the measured EDMR signal remains challenging. A range of reports ascribed the signal to either V_{Si}[51,112–114] or to carbon dangling bonds (P_{bC}).[110,115,116] These defect assignments are based on comparisons of the g-factor and hyperfine values with theoretical descriptions. The discrepancies between these reports may be due to differences in the measured devices or even the experimental parameters employed. This certainly suggests the need for careful experiments when faced with such inconsistencies.

Nonetheless, EDMR techniques are expected to find broad application in a number of QT applications. Energy level shifts of spin sublevels are an extremely sensitive probe of magnetic fields,[51,117] electric fields, and temperature. Therefore, spin resonance techniques may form the basis of emerging quantum sensing and metrology applications.

B. Optically detected magnetic resonance

The optical version of EDMR, optically detected magnetic resonance (ODMR), combines PL measurements with magnetic resonance methods. The measurement requires a PL spectrometer or sensitive photon detectors. As with EDMR, a MW generator and a method to supply the sample with the MW field such as an antenna or resonator are required. An advantage of ODMR over EDMR is, of course, that no device fabrication is required and that the measurement can be performed at any stage of device processing. Single defects in as-grown crystals can be detected with this technique as it is as sensitive as the optical techniques described above. ODMR can be integrated with confocal microscopy for spatially resolved measurements. In doing so, both ensemble and single defect level measurements can be accomplished.

The mechanism on which ODMR is based is distinct from EDMR. As an example, the ground state energy level diagram of the V_{Si}^-, a spin $S = 3/2$ defect in 4H-SiC, is shown in Fig. 9(a).[91,118,119] As a magnetic field is applied along the c-axis, the energy levels split according to the Zeeman effect. The spin-dependent recombination process is different from EDMR. For V_{Si}, the $m_s = \pm 1/2$ states are preferentially populated during laser excitation. This optical pumping polarizes the spins. The PL intensity is lower when the spins are in the $m_s = \pm 1/2$ states and greater when in the $m_s = \pm 3/2$ states. When RF energy is applied in resonance with allowed spin transitions, the spin populations are redistributed and the PL intensity will increase. This increase is small (typically 0.02%) so lock-in methods again are helpful. The magnetic field at which this occurs vs the RF frequency is shown in Fig. 9(b). The 70 MHz zero field splitting observed for V_{Si}^- is a unique fingerprint for this defect and can be used for the purposes of defect identification.

Leveraging the pioneering quantum experiments on the NV center in diamond, SiC defects have recently been assessed for their suitability for QT applications.[9,23,120] Both V_{Si} and $V_{Si}V_C$ have been assessed for quantum sensing applications.[119,121–124] Importantly, single defect spin control has been demonstrated for both V_{Si}[119,125]

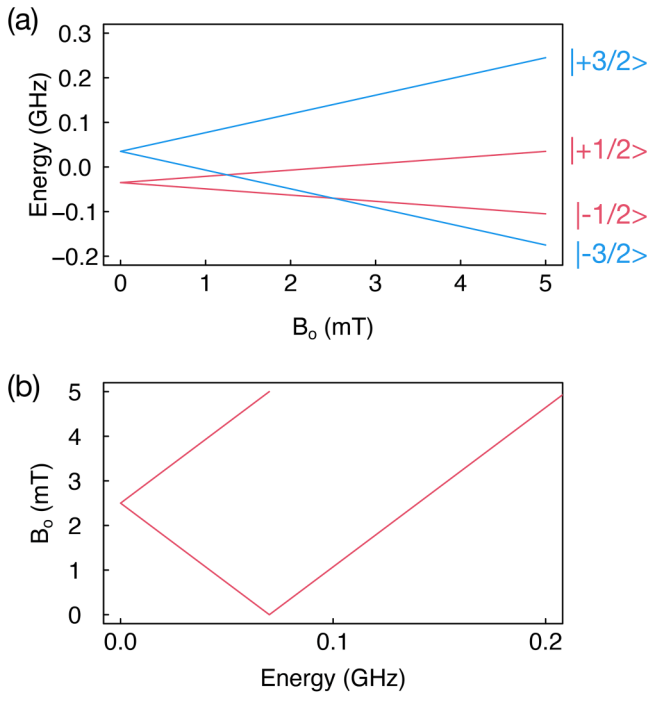

FIG. 9. (a) The calculated ground state energy level structure of the V_{Si} defect in 4H-SiC as a function of magnetic field applied along the c-axis.[118] It consists of both the $m_s = \pm 1/2$ and $m_s = \pm 3/2$ spin sub-levels. (b) The expected field at which MW resonance occurs in an ODMR measurement. A 70 MHz zero field splitting is clearly observed at zero magnetic field.

and $V_{Si}V_C$.[121] These defects have optical transitions that are spin-selective permitting quantum state readout with high fidelity. By virtue of these properties, the dipolar coupling with Si nuclear spins can be measured and used to perform quantum operations or as quantum memory.[126,127] Indeed, the coherence time of the electron spin in V_{Si} is quite long, up to 20 ms at 20 K[128]—ample time to perform various spin control operations. We certainly expect further innovations and profound insights in this field given the current pace and global investment in QT.

The optical excitation combined with electrical detection is also a possibility. This technique makes use of a spin-dependent photo-ionization mechanism and has been demonstrated for V_{Si}.[129] Electrical devices are required and can be designed to address small SiC volumes within the device. Such a technique is important for QT since it allows high sensitivity electronics to be leveraged and may enable single-shot electrical spin readout as demonstrated with the $V_{Si}V_C$.[130] Such capabilities are central to entanglement distribution for quantum networks.

VI. COMPLEMENTARY TECHNIQUES

There are an extremely diverse range of techniques available to study the properties of defects in SiC. Many fall outside the categories we have defined above. In this section, we discuss a number of other important (in our opinion) techniques that present unique opportunities to understand SiC defects and devices in new and useful ways. This includes the edge transient-current technique (edge-TCT), muon spin rotation spectroscopy as well as the complementary theoretical methods that are often employed alongside experiments.

A. Edge-TCT

The generation of electron–hole pairs by laser or ion excitation of carriers across the bandgap of SiC can be used to simultaneously map the carrier dynamics, carrier-trap interactions, and device functionality. Such techniques draw upon the ability to scan the excitation beam over the sample to build up a 2D or even a 3D map of the device. This includes techniques like laser beam induced current (LBIC), electron beam induced current (EBIC), the ion beam counterpart (IBIC), and the edge transient-current technique (edge-TCT). The latter was initially developed for the investigation of silicon particle detectors[131] but can be applied to wide bandgap semiconductors to make inferences about the defect distribution within the bulk, as shown recently for diamond.[132] Edge-TCT involves exciting a spatially confined cloud of free electron–hole pairs in the bulk of a device with a pulsed laser and measuring the transient current these carriers induce when they drift through the device in an externally applied electric field. This current is amplified by a broadband amplifier and recorded by a laser triggered oscilloscope. To enhance the signal to noise ratio, several (usually 20) transient current traces are acquired for each coordinate in a 2D or 3D scan.

The excitation source can be a pulsed (pico- or femtosecond) laser or single ionizing particles.[133] Both methods result in a highly localized region where charge carriers are created. This enables the mapping capability of the technique. Figure 10 shows a schematic of the edge-TCT setup. A pulsed laser beam enters the device through a polished edge (hence the name edge-TCT) and excites charge carriers at a known distance from the top and bottom electrodes. The sample can be placed on a xyz stage to build maps of the transient current response of the device—very much like the PL mapping technique described in Fig. 7.

Above bandgap light can be used to excite the free carriers. The wavelength may be varied to change the penetration depth. Improved spatial resolution can be achieved by using an intense femtosecond laser with a sub-bandgap energy. Multiphoton absorption processes, where the electron is lifted in the conduction band via consecutive virtual states, will occur at the focal point of

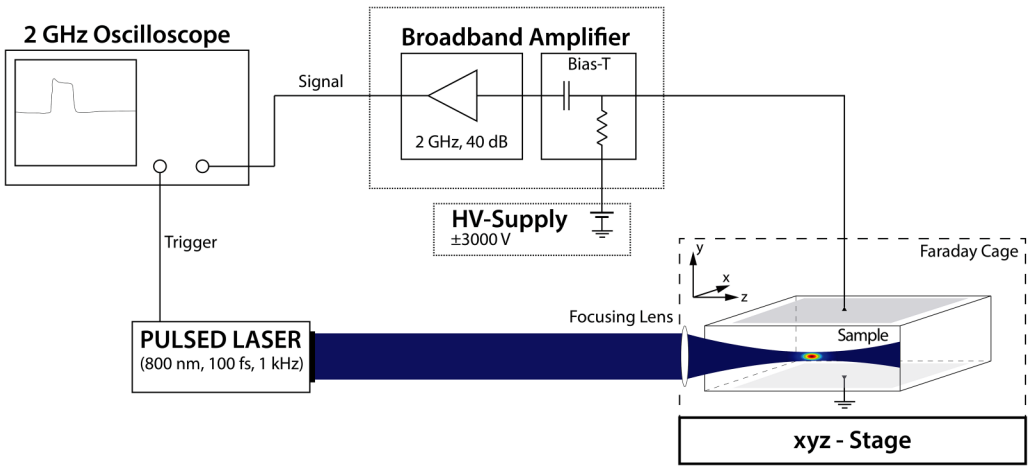

FIG. 10. Schematic of a multi-photon absorption edge-TCT setup. The pulsed laser that is focused into the device through the device edge only excites charge carriers in the focal point.

the laser as schematically shown in Fig. 10. This allows 3D mapping capabilities. The lateral scan resolution is about 1 μm for a 800 nm wavelength laser.

The measured transient current pulses provide information about the electron and hole drift velocities, the charge collection efficiency in the bulk, the electric field in the bulk, and an estimation of the amount of trapped charge carriers.

From the width of the pulses and the distance to the electrodes, the drift speed for electrons and holes can be calculated. If done at different bias voltages, the mobilities of electrons and holes can be extracted from these measurements.

The total integrated signal gives a value of the collected charge allowing charge collection efficiency maps to be formed. In good quality devices, high enough fields, and sufficiently long integration times, it is not unusual to collect all excited carriers in the active region of the device (100% charge collection efficiency). In areas of the device filled with defects, however, the trapping times of the carriers can exceed the acquisition time of the current pulses and a deficit of charge is measured. In addition to trapping at defects, space charge originating from electrically charged defects in the device can drastically reduce the amount of collected charge by locally shielding the externally applied electric field and thus promoting recombination and trapping effects. Thus, edge-TCT is an intriguing technique for correlating defective regions in the material with device functionality.

Figure 11 shows the charge collection map of a -200 V reverse biased circular Schottky contact on SiC with a diameter of 700 μm. The Schottky contact is on the top surface at y $= \mu$m. Note that the measurement between y $= -20\,\mu$m and y $= 0\,\mu$m is biased by beam loss at the edge of the sample. This can in theory be avoided by moving the electrodes to the edge of the sample.

Modifications to the measured device or how the measurement is made can be explored to enhance the defect spectroscopy capabilities of the edge-TCT technique. Examples include measurements at different sample temperatures or during illumination of the sample with light of a specific wavelength. These two methods would allow only certain defects to be probed depending on their energy levels in the bandgap.

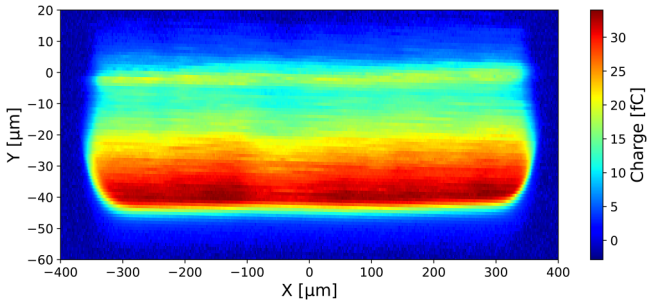

FIG. 11. Charge collection map of a reverse biased Schottky contact on SiC. The Schottky contact is located at y $= 0\,\mu$m while the substrate side of the sample starts at y $= -440\,\mu$m and is not shown in this plot. The resolution of the scan is dx $= 2\,\mu$m and dy $= 1\,\mu$m.

B. Muon spin rotation spectroscopy

The interactions between matter and elementary particles such as muons, electrons, or positrons can provide unique information about the properties of defects in semiconductors. In a muon spin rotation (μSR) experiment, the charge and spin of a muon are used as sensitive local electronic and magnetic probes. This technique has been extensively used in areas such as superconductivity, radical chemistry, and material science by leveraging the muons as magnetic spin micro-probes, but can also be employed as a powerful tool for studying defects and carrier distributions in semiconductors.

A major advantage of μSR compared to other non-destructive particle beam methods is its applicability to a wide range of materials. Unlike nuclear magnetic resonance (NMR), μSR does not require specific target nuclei nor does it rely on a thermal equilibrium spin polarization (and hence necessitating low temperatures and high magnetic fields) as it is known from ESR. A comparable method is positron-annihilation spectroscopy (PAS), but while PAS is selectively sensitive to vacancy defects, muon spin rotation can be employed to study a wide range of semiconductor defects.

The working principle of a μSR measurement is depicted in Fig. 12(a): perfectly spin-polarized muons (in most cases μ^+) with a well-defined kinetic energy are implanted into the material of interest where they quickly lose energy, adopt interstitial lattice sites, and thermalize without significant loss of polarization. In the presence of a magnetic field applied perpendicular to the initial muon polarization, the precession frequency of the muon spin is then the vector sum of the applied field and any local field present in the sample. After a mean lifetime of 2.2 μs, the muons decay into a positron e^+ (or an electron in the case of μ^-) and two neutrinos. Due to parity violation, the positrons are preferentially emitted along the direction of the muon spin at the time of the decay. With detectors placed around the sample, the asymmetry of the muon decay along different directions as a function of time, $A(t)$, is measured and contains information on the hyperfine interaction between the muon and the electrons in the target material [Fig. 12(b)].

In semiconductors and insulators, the implantation of μ^+ leads to the formation of a hydrogen-like bound state called Muonium [$Mu^0 = (\mu^+ e^-)$], which can be distinguished from the unbound μ^+ by its larger precession frequency around the applied magnetic field. The amplitudes of the diamagnetic and paramagnetic precession signals A_D and A_{Mu} are proportional to the fraction of muons in that particular state (F_D and F_{Mu}, respectively, following the convention used in the literature), which are characteristic parameters for each material system. Different doping levels as well as the presence of defects or extended crystal damage can influence electron capture and charge exchange processes of the implanted muon and with that the fraction of Mu^0 formed in the host material. By measuring the asymmetries as a function of temperature and the applied magnetic field, information on the muon's electronic environment can be obtained.

Due to the resemblance of the muonium to the hydrogen atom, μSR has been primarily employed to study hydrogen-like impurities in a broad range of materials such as Si, Ge, diamond, group (III-V),

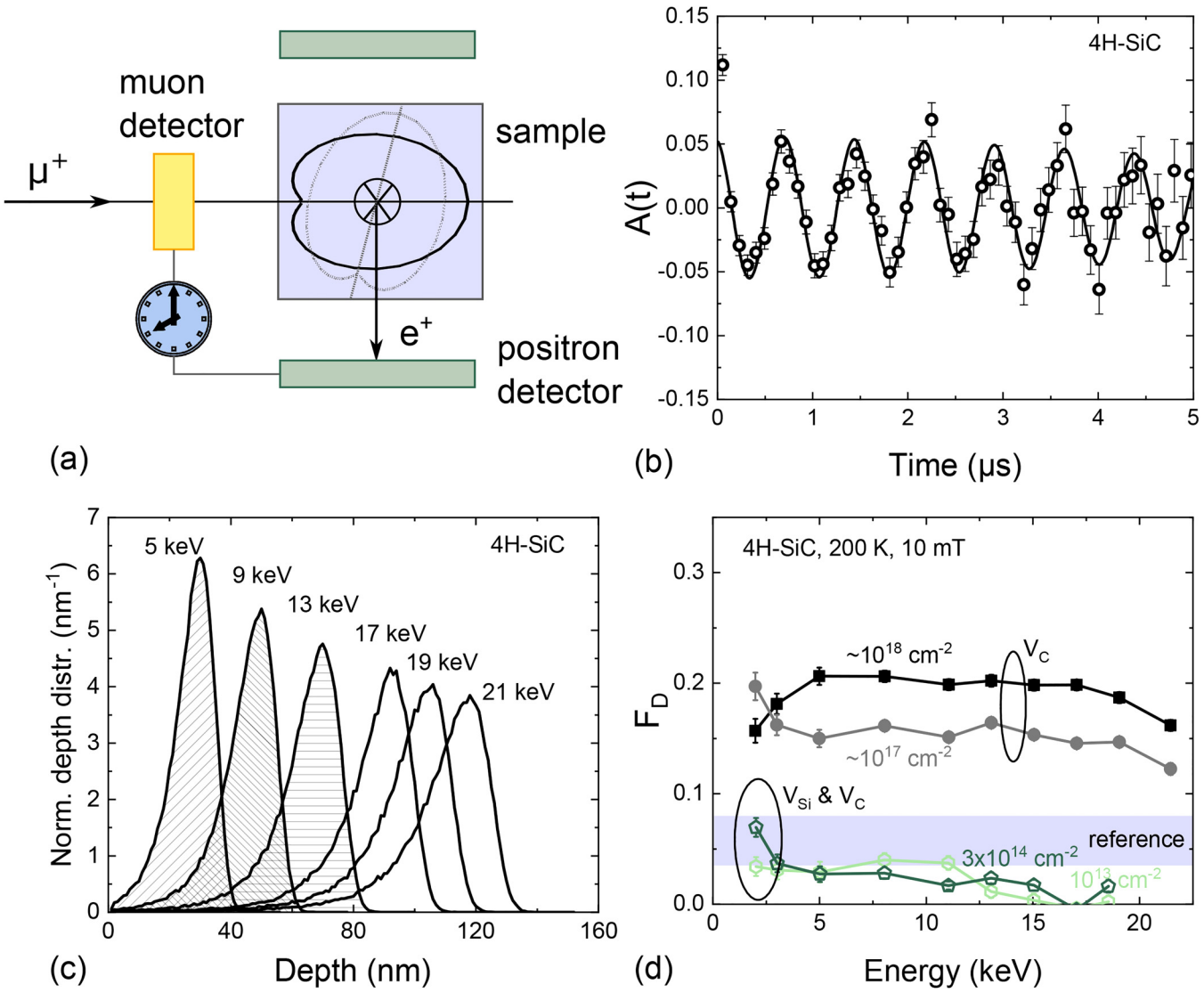

FIG. 12. (a) Muon spin rotation setup. (b) Raw histogram of the detected positron counts for where the radioactive exponential decay has already been removed. (c) Muon implantation profiles in 4H-SiC for energies between 5 and 21 keV. (d) Diamagnetic fraction of proton-irradiated 4H-SiC with varying V_{Si} and V_C concentrations.

and (II-VI) semiconductors as well as different oxides.[134–136] In addition, a variety of defects have been investigated, including vacancy defects in silicon and diamond, as well as irradiation-induced defects in Si, Ge, and GaAs.[134,137,138]

One drawback of conventional muons used in μSR is their large kinetic energies: muons that originate from pion decay at proton accelerators have energies around 4 MeV, resulting in muon probe depths around 0.1–1 mm. This limits their applicability to standard bulk samples. At dedicated low-energy muon (LEM) facilities (currently only available at the Paul Scherrer Institute, Switzerland) on the other hand, the muons are moderated down to energies in the keV range, allowing depth-resolved studies of thin films and multilayered structures in the first ∼ 200 nm of the material [Fig. 12(c)].

In SiC, low-energy muons have been successfully employed to study vacancy defects upon proton irradiation as well as oxidation-induced defects at the SiC/SiO_2 interface. In the case of vacancy defects, experiments on proton-irradiated and subsequently annealed 4H-SiC show a distinct difference in the muon response to V_{Si} compared to V_C,[98,139] suggesting that LE-μSR is sensitive to the different relaxation mechanisms driven by the vacancy nearest-neighbor dangling bonds. As summarized in Fig. 12(d), samples with very large V_C concentrations ($> 1 \times 10^{17}$ cm^{-3}) exhibit an increased diamagnetic fraction at the expense of F_{Mu} compared to

non-irradiated SiC (blue shaded area). In contrast, samples annealed at lower temperatures where the V_{Si} is still present show a smaller F_D compared to the non-irradiated reference sample, indicating that hardly any diamagnetic Mu^+ or Mu^- is formed. Interestingly, a change in the diamagnetic signal is already observed at very low V_{Si} concentrations in the 1×10^{14} cm^{-3} to 1×10^{15} cm^{-3} range, much lower than what is required for affecting F_D with the V_C-rich samples. This difference may be partially explained by the larger Si void compared to V_C, but is mainly attributed to the strong attractive force of negatively charged V_{Si} for the positive muon and the larger energy gain by the formation of V_{Si}-Mu compared to V_C-Mu.

In the case of thermally oxidized SiC, the impact of oxidation-induced defects on the muonium formation process has been shown. Depth profiles across the SiC/SiO_2 interface revealed an extended region of around 10–30 nm—both on the oxide and on the semiconductor side—with a larger diamagnetic fraction.[140] For deposited oxides, on the other hand, no variation of F_D near the interface is observed. Although the exact mechanism is still not fully understood, the increase of F_D may be explained by large densities of electrically active defects directly at the interface, as well as crystal distortions caused by C interstitial injection into the SiC substrate in an extended region around the interface. At the moment, a contribution of oxidation-induced strain across the interface cannot be ruled out. In summary, these findings on the interactions of near surface defects in SiC with the implanted muons underline the potential of LE-μSR to enhance our understanding of both the defects themselves, but also their interaction with various device types.

C. Theoretical methods

Optical and electrical characterization techniques have, as outlined above, been used extensively for studying defects in SiC. A substantial amount of information is required about a specific defect signal to reveal its identity. Thus, it is often necessary to correlate different characterization techniques and vary experimental parameters such as irradiation and temperature to gain insight into defect properties. Despite all these possibilities, unambiguous defect identification can still be a challenge. Theoretical methods that predict defect properties given the proposed atomic structure is an excellent complement to experimental results, offering insight that may aid in the interpretation of experimental data, and ultimately lead to the identification of a defect's atomic structure.

A number of methods have been developed to achieve this. The most commonly employed for defects in SiC is density functional theory (DFT). DFT is a self-consistent field method to iteratively solve the Schrödinger equation and obtain the total energy of a system. The defect to be studied is defined by constructing a *supercell* containing the defect (or other systems) and the surrounding material. The supercell is then repeated in three dimensions using periodic boundary conditions. Even for relatively large supercells with >500 atoms, this approach will typically emulate a defect concentration in the 10^{18}–10^{21} cm^{-3} range. In other words, DFT calculations provide predictions for defect densities that are often well beyond the dilute limit that is probed using various characterization techniques. Hence, to ensure good agreement between DFT calculations and experimental techniques, it is vital to choose calculation parameters that minimize the interactions between the periodically repeated supercell defects (this is particularly important for charged systems). An example defective structure is shown in Fig. 13 for the case of V_{Si}^- in 4H-SiC.

DFT calculations rely on an exchange-correlation (XC) functional to approximate the electronic interactions in a material. The so-called local and semi-local functionals based on the local density approximation (LDA) and generalized gradient approximation (GGA) are useful but suffer from consistent under-estimation of the semiconductor bandgap. This, in turn, affects the accuracy of predictions related to the electronic structure of materials including defect energy levels. More recently, hybrid functionals that incorporate a portion of screened Hartree-Fock exact exchange have become popular. These go a long way in canceling the self-interaction error of the LDA and GGA functionals and have yielded excellent results for both semiconductor bandgaps and defect energetics.[141–143]

An important result of DFT calculations in the context of semiconductor defects is the defect formation energy diagram,[143–145] which portrays the formation energy of a defect in different charge states with respect to the Fermi level of the semiconductor. The formation energy of a defect X in the charge state q is calculated as

$$E^f[X^q] = E_{\text{total}}[X^q] - E_{\text{total}}[\text{bulk}] - \sum_i n_i\mu_i + qE_F + E_{\text{corr}}. \quad (1)$$

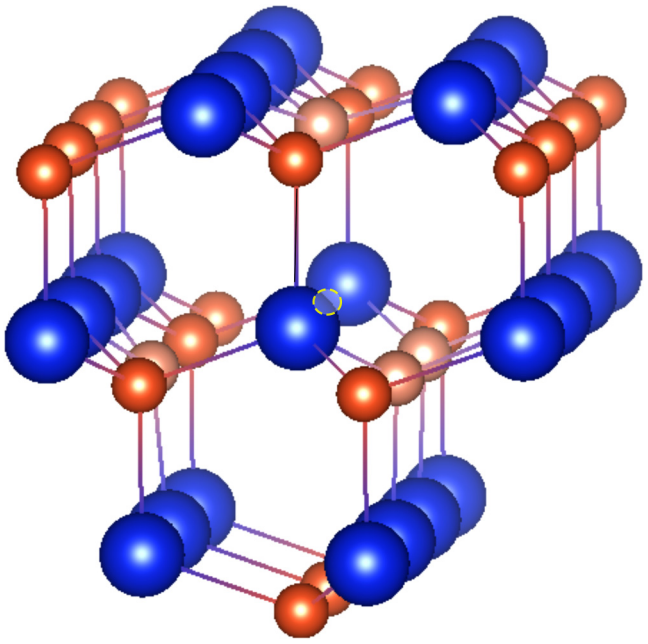

FIG. 13. Defect geometry predicted by DFT calculations for the V_{Si}^- in 4H-SiC with Si atoms in blue and C in orange. The figure shows the defect-induced displacement of nearest neighbor atoms (lighter orange) and highlights the symmetry of the defect, in this case C_{3v}.

Here, $E_{\text{total}}[X^q]$ and $E_{\text{total}}[\text{bulk}]$ are the total energies of the supercell with and without the defect, respectively, n_i is the number of atoms of species i that are added ($n_i > 0$) or removed ($n_i < 0$) to form the defect, μ_i is the chemical potential, E_F is the Fermi level, and E_{corr} is a correction term to account for charged defects. The formation energy translates into a defect concentration in the material as a function of growth or annealing conditions and can be compared to experimental techniques such as DLTS. Furthermore, the thermodynamic transition levels of electrically active defects can be extracted, corresponding to thermal ionization energies that are observed in experiments such as DLTS and EPR.

The success of utilizing DFT to interpret experimental results can be exemplified by the identification of the $Z_{1/2}$ level commonly observed in DLTS spectra of n-type 4H-SiC. By combining photo-EPR, DLTS measurements, and DFT calculations, the $Z_{1/2}$ level was assigned to the (0/2-) charge-state transition level of the carbon vacancy in 4H-SiC, which was simultaneously identified as a negative-U transition[14]—marking the $Z_{1/2}$ level as a prominent charge carrier trap and recombination center. Formation energy diagrams for the V_C are shown in Fig. 14, highlighting features such as the low formation energy of the V_C enabling thermal defect formation, the charge transition levels, and the negative-U characteristics of the (0/2-) transition. Later works have utilized the synergy between theory and experiment to perform similar but tentative identifications of the DLTS peaks labeled S1/S2, EH_4/EH_5, and the M-center to the V_{Si},[146] the $C_{Si}V_C$,[147] and the C split-interstitial,[148] respectively.

A crucial aspect when incorporating defect functionalities in device design (e.g., removal of V_C for power devices or inclusion of V_{Si} for QT) is to understand the defect response to common

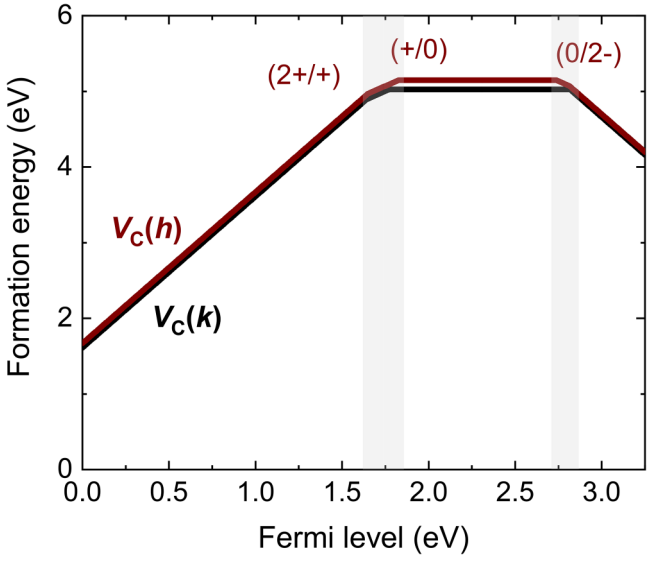

FIG. 14. Formation energy diagram for the carbon vacancy (V_C) in 4H-SiC. The abbreviations *h* and *k* refer to the vacancy being located at the hexagonal and quasi-cubic lattice sites of the 4H polytype, respectively. Based on data from Ref. 139.

fabrication processes such as irradiation and annealing. Elevated temperatures can cause migration of defects and dopants and transformation into different defect types. The nudged elastic band (NEB) method[149] combined with DFT calculations is commonly used to study defect dynamics in semiconductor materials, but also molecular dynamics and Monte Carlo simulations can be used to this end. For example, the diffusion of the V_C has been studied extensively to understand its stability and facilitate V_C removal.[61,150,151] Combining theory and experiment revealed that the V_C is expelled from 4H-SiC material at temperatures $\geq$1600 °C via single atomic hops on the C sub-lattice. Interestingly, migration of the V_C is anisotropic in 4H-SiC with faster diffusion along the basal direction within the hexagonal (*h*) lattice plane compared to all other directions.[152] A similar directional dependence was found for the V_{Si} in n-type 4H-SiC using Monte Carlo simulations.[153]

Another classic example is the energetically favorable transition of the V_{Si} into the $C_{Si}V_C$, which merely requires the movement of a carbon atom into the V_{Si} position. The V_{Si} and $C_{Si}V_C$ are stable in different Fermi level ranges, with the former being mainly found in n-type and the latter in p-type 4H-SiC.[75,154] The Fermi level dependence of the competition between transformation between the V_{Si} and $C_{Si}V_C$ and migration of isolated defects was recently studied using DFT calculations,[155] marking the versatility and importance of combining theory and experiment for defect studies.

First-principles calculations are an important tool for revealing and functionalizing also the quantum compatible properties of quantum emitters and spin centers in SiC (see, e.g., Ref. 156 for an overview of DFT calculations for QT). Despite initially being a 0 K and ground state only technique, recent developments have enabled the study of optical- and spin-dependent processes along with phonon involvement. To estimate the ZPL for single-photon emission, for instance, the calculated single-particle energy levels provide a useful glimpse into electronic orbital occupations,[157] or more accurate estimates of the ZPL energy can be made using the Δ self-consistent field (Δ-SCF) method.[158] Identifying the emitter responsible for an optical fingerprint is crucial to employ them in QT devices. Prominent examples of such identification aided by theory include zero phonon line estimates for the different lattice configurations of V_{Si}^- and $V_{Si}V_C^0$ in 6H-[159] and 4H-SiC.[92] Moreover, DFT calculations are increasingly being used to predict the full emission spectrum from a defect center, as demonstrated for, e.g., the NV^- center in diamond[160] and more recently the V_{Si}^- in 4H-SiC.[161] Local vibrational modes[162] and interactions between excited states and strain[163] and electrical fields[164] have also been investigated for the case of V_{Si}.

DFT calculations are often employed to understand the magnetic properties of defects and complement experimental techniques such as EPR and ODMR. First-principles estimates of hyperfine parameters, *g* tensors, and the zero-field splitting (ZFS) have aided in identifying the chemical nature and structure of paramagnetic defects detected with these techniques, as exemplified by the use of ZFS calculations to identify the N_CV_{Si} center in SiC by EPR.[28]

VII. COMPARISON OF TECHNIQUES

As can be seen above, there are a diverse range of techniques available. Each probes a distinct aspect of the defect and is

accompanied by a unique set of pros and cons. A number of key factors that may influence which technique is applied may include sensitivity, device/material requirements, and the complexity of the experimental apparatus and of the data interpretation. This last point is especially of concern when relying on methods developed for other materials than SiC. We summarize the main techniques mentioned above in Table II with these key metrics in mind.

Combining these techniques in some way is a powerful approach for defect identification or developing a description of how a defect may impact a particular technology. Techniques such as EDMR or ODMR combine electrical or optical measurements with traditional magnetic resonance techniques to form a highly sensitive defect probe. As indicated in Table II, the sensitivity is enhanced by over eight orders of magnitude compared to traditional ESR. These methods have, thus, become the basis of a broad range of QT applications such as quantum sensing. At the same time, methods have been developed to apply these same techniques to power electronics applications and on a level that will be applicable to production line quality control measurements.[165]

Equally important perhaps are synergistic efforts that correlate the results from different techniques. This has been a key approach for defect identification and to elucidate the atomic origin of a signal for a specific technique. Magnetic resonance techniques are often used to define the defect symmetry. First-principles calculations are then applied to confirm hyperfine characteristics and spin quantum numbers for a likely candidate defect. By varying the concentration of a defect in a series of samples, signal strengths from other techniques can be correlated together. Of course, some caution is required to avoid false correlations.

The dominant PL bands observed after irradiation of SiC were proposed to emanate from the V_{Si} defect based on the number of ZPLs in each polytype, the corresponding hyperfine characteristics determined via ODMR and comparisons to EPR measurements and theory.[76] After this early work, the character of the signals continued to be refined. It is now firmly established that these signals are from the negatively charged silicon vacancy, V_{Si}^{-}, with $S = 3/2$.[166] Similarly, the $V_{Si}V_C$ defect was identified with a combination of EPR measurements and theory.[105] This allowed the development of a detailed picture of the defect evolution during annealing.[84] A description of the spin properties of these two defects continues to be developed for possible applications in QT.[77]

In the context of SiC devices, the hitherto most sought after defect identification was that of the lifetime limiting $Z_{1/2}$ center in 4H-SiC. Using both EPR and DLTS, together with DFT calculations, the $Z_{1/2}$ level was assigned to the (2-/0) charge-state transition of V_C[14] at h and k lattice sites.[167] This important identification prompted several studies into targeted V_C removal based on these initial insights.[168,169]

Many traditional electrical techniques are able to quantify the defect density at the SiC/SiO_2 interface yet the atomic identity remains elusive. Recent developments have seen the application of single defect optical spectroscopy to characterize these defects.[44] In the case of these optically active defects, magnetic resonance techniques were not able to extract further information suggesting that the transitions involved spinless states only. This may make defect identification more challenging but there are ample opportunities to correlate their properties with perhaps more exotic techniques such as muon spectroscopy. These could prove crucial for finally understanding the interface and its defects to improve SiC based power electronic devices.

There are a raft of other defects that remain unidentified which may be useful for certain applications once their properties are described further. The synergistic examples mentioned here have proven to be quite profitable and are an efficient route toward understanding defects in SiC as discussed further in Sec. VIII.

VIII. OUTLOOK AND OPPORTUNITIES

SiC MOSFETs are now commercialized and seeing rapid growth in the high power industry. These applications demand relatively extreme performance from these devices which truly leverages the favorable thermal and electronic properties of SiC. This has, in turn, placed further demands on defect characterization work which to a large extent guides improvement in device performance. Most work in this context has benefited greatly from the decades of research into Si electronics. Like Si, many of the industrial fabrication processes are similar and SiC is also able to form a native dielectric layer on its surface. However, since SiC is a much

TABLE II. Overview of the different techniques discussed herein.

Category	Technique	Device	Sensitivity	Defect type
Electrical	CV(Hi-Lo)	MOS	10^{10}–10^{12} cm^{-2} eV^{-1}	SiC/SiO_2
	$C\Psi_s$	MOS	$>10^{11}$ cm^{-2} eV^{-1}	SiC/SiO_2
	CP	MOSFET	$>10^{11}$ cm^{-2} eV^{-1}	SiC/SiO_2
	DLTS	Junction	$>10^{10}$ cm^{-2} eV^{-1}	Bulk or SiC/SiO_2
	TAS	Junction		Bulk
Optical	PL	No device	One defect	Bulk or SiC/SiO_2
Magnetic	ESR	No device	$>10^{10}$ spins	Bulk or SiC/SiO_2
	EDMR	Junction	<100 spins	Bulk or SiC/SiO_2
	ODMR	No device	One spin	Bulk
Other	Edge-TCT	Junction	?	Bulk
	μSR	No device	$>10^{14}$ cm^{-3}[a]	Near surface

[a]The sensitivity is defect dependent: $>10^{14}$ cm^{-3} for V_{Si} and $>10^{17}$ cm^{-3} for V_C.

more complicated material more traditional techniques must be tailored to SiC and we find new techniques are being developed to gain a better understanding of defects in this fascinating material.

In parallel, recent successes with the control and readout of spin defects in SiC are making a significant impact on emerging QT. This field draws heavily on methods developed for the NV center in diamond and also traditional ESR techniques. The goal in this Perspective was to look at both fields side-by-side, identify similarities and places where there could be new opportunities by combining know-how from the two. This is particularly fertile ground when considering the electrical readout of spins in SiC, leveraging the amazing developments in SiC electronics in recent years. Conversely, characterization techniques from the QT field allow one to address defects on the single defect level, thereby promoting insight into defect properties that may otherwise be obscured by an ensemble average.

In identifying the atomic structure of defects in SiC, the most successful experiments usually combine several techniques in addition to insight from the theoretical perspective. In this sense, ODMR and EDMR are particularly powerful since they are able to gain information on the symmetry of a defect while also probing its electrical or optical properties. They are equally suited to quantification of defect densities and we may soon see these "quantum"-related techniques being applied in the power electronics industry. This then allows us to identify more processing strategies to more efficiently create or annihilate the target defect. Furthermore, electronic devices are likely to play a more prominent role in the QT field moving forward since they may host more scalable quantum architectures similar to phosphorus in silicon qubit devices.[170] We can expect that both SiC power electronics and SiC QT will continue to develop rapidly. Defect characterization techniques are common ground and a way to enhance cross-pollination between these two quite different fields. So far, QT has greatly benefited from developments in the power electronics field through improvements in wafer scale high-quality materials and device processing protocols. We expect findings in QT will also make an impact on SiC devices and indeed generate new technologies.

ACKNOWLEDGMENTS

B.C.J. acknowledges the Australian Research Council Centre of Excellence for Quantum Computation and Communication Technology (No. CE170100012). M.E.B. acknowledges support by an ETH Zürich Postdoctoral Fellowship.

AUTHOR DECLARATIONS

Conflict of Interest

The authors have no conflicts to disclose.

DATA AVAILABILITY

The data that support the findings of this study are available from the corresponding author upon reasonable request.

REFERENCES

[1]X. Guo, Q. Xun, Z. Li, and S. Du, "Silicon carbide converters and MEMS devices for high-temperature power electronics: A critical review," Micromachines **10**, 406 (2019).
[2]*Wide Bandgap Semiconductors for Power Electronics*, Semiconductors and Semimetals, 1st ed., edited by P. Wellmann, N. Ohtani, and R. Rupp (Wiley-VCH, Weinheim, 2021).
[3]N. T. Son, C. P. Anderson, A. Bourassa, K. C. Miao, C. Babin, M. Widmann, M. Niethammer, J. Ul Hassan, N. Morioka, I. G. Ivanov, F. Kaiser, J. Wrachtrup, and D. D. Awschalom, "Developing silicon carbide for quantum spintronics," Appl. Phys. Lett. **116**, 190501 (2020).
[4]S. Castelletto and A. Boretti, "Silicon carbide color centers for quantum applications," J. Phys.: Photonics **2**, 022001 (2020).
[5]M. E. Bathen and L. Vines, "Manipulating single-photon emission from point defects in diamond and silicon carbide," Adv. Quantum Technol. **4**, 2100003 (2021).
[6]S. Castelletto, B. C. Johnson, V. Ivády, N. Stavrias, T. Umeda, A. Gali, and T. Oshima, "A silicon carbide room-temperature single-photon source," Nat. Mater. **13**, 151–156 (2014).
[7]A. Lohrmann, B. C. Johnson, J. C. McCallum, and S. Castelletto, "A review on single photon sources in silicon carbide," Rep. Prog. Phys. **80**, 034502 (2017).
[8]J. B. S. Abraham, C. Gutgsell, D. Todorovski, S. Sperling, J. E. Epstein, B. S. Tien-Street, T. M. Sweeney, J. J. Wathen, E. A. Pogue, P. G. Brereton, T. M. McQueen, W. Frey, B. D. Clader, and R. Osiander, "Nanotesla magnetometry with the silicon vacancy in silicon carbide," Phys. Rev. Appl. **15**, 064022 (2021).
[9]D. D. Awschalom, R. Hanson, J. Wrachtrup, and B. B. Zhou, "Quantum technologies with optically interfaced solid-state spins," Nat. Photonics **12**, 516–527 (2018).
[10]G. Zhang, Y. Cheng, J.-P. Chou, and A. Gali, "Material platforms for defect qubits and single-photon emitters," Appl. Phys. Rev. **7**, 031308 (2020).
[11]V. A. Norman, S. Majety, Z. Wang, W. H. Casey, N. Curro, and M. Radulaski, "Novel color center platforms enabling fundamental scientific discovery," InfoMat **3**, 869–890 (2021).
[12]Here, the subscript refers to the atomic site and the normal text is what occupies the site.
[13]K. Danno, D. Nakamura, and T. Kimoto, "Investigation of carrier lifetime in 4H-SiC epilayers and lifetime control by electron irradiation," Appl. Phys. Lett. **90**, 202109 (2007).
[14]N. T. Son, X. T. Trinh, L. S. Løvlie, B. G. Svensson, K. Kawahara, J. Suda, T. Kimoto, T. Umeda, J. Isoya, T. Makino, T. Ohshima, and E. Janzén, "Negative-*U* system of carbon vacancy in 4*H*-SiC," Phys. Rev. Lett. **109**, 187603 (2012).
[15]N. Iwamoto and B. G. Svensson, "Point defects in silicon carbide," in *Defects in Semiconductors*, Semiconductors and Semimetals Vol. 91, edited by L. Romano, V. Privitera, and C. Jagadish (Elsevier, 2015), Chap. 10, pp. 369–407.
[16]H. Amini Moghadam, S. Dimitrijev, J. Han, and D. Haasmann, "Active defects in MOS devices on 4H-SiC: A critical review," Microelectron. Reliab. **60**, 1–9 (2016).
[17]U. Grossner, J. K. Grillenberger, J. Woerle, M. E. Bathen, and J. Mueting, "Intrinsic and extrinsic electrically active point defects in SiC," in *Wide Bandgap Semiconductors for Power Electronics: Materials, Devices, Applications*, Semiconductors and Semimetals Vol. 91, edited by P. Wellmann, N. Ohtani, and R. Rupp (Wiley-VCH, Weinheim, 2021), Chap. 6, pp. 137–168.
[18]N. Ohtani, "Dislocation formation during physical vapor transport growth of 4H-SiC crystals," in *Wide Bandgap Semiconductors for Power Electronics: Materials, Devices, Applications*, Semiconductors and Semimetals Vol. 91, edited by P. Wellmann, N. Ohtani, and R. Rupp (Wiley-VCH, Weinheim, 2021), Chap. 1, pp. 3–32.
[19]A. M. Jakob, S. G. Robson, V. Schmitt, V. Mourik, M. Posselt, D. Spemann, B. C. Johnson, H. R. Firgau, E. Mayes, J. C. McCallum, A. Morello, and D. N. Jamieson, "Deterministic single ion implantation with 99.87% confidence for scalable donor-qubit arrays in silicon," Adv. Mater. **34**, 2103235 (2022).
[20]O. V. Losev, "Luminous carborundum detector and detection with crystals," in *Wireless Telegraph and Telephone* (Forgotten Books, 1924), Vol. 26, p. 403.
[21]O. V. Losev, Philos. Mag. **6**, 1024–1044 (1928).
[22]O. V. Losev, Soviet patent 12191 (31 December 1929); N. Zheludev, "The life and times of the LED—A 100-year history," Nat. Photonics **1** 189–192 (2007).

[23]G. Wolfowicz, F. J. Heremans, C. P. Anderson, S. Kanai, H. Seo, A. Gali, G. Galli, and D. D. Awschalom, "Quantum guidelines for solid-state spin defects," Nat. Rev. Mater. **6**, 906–925 (2021).
[24]J. Casady and R. Johnson, "Status of silicon carbide (SiC) as a wide-bandgap semiconductor for high-temperature applications: A review," Solid-State Electron. **39**, 1409–1422 (1996).
[25]P. B. Klein, B. V. Shanabrook, S. W. Huh, A. Y. Polyakov, M. Skowronski, J. J. Sumakeris, and M. J. O'Loughlin, "Lifetime-limiting defects in n^- 4H-SiC epilayers," Appl. Phys. Lett. **88**, 052110 (2006).
[26]M. W. Doherty, N. B. Manson, P. Delaney, F. Jelezko, J. Wrachtrup, and L. C. Hollenberg, "The nitrogen-vacancy colour centre in diamond," Phys. Rep. **528**, 1–45 (2013).
[27]R. A. Parker, N. Dontschuk, S.-I. Sato, C. T.-K. Lew, P. Reineck, A. Nadarajah, T. Ohshima, B. C. Gibson, S. Castelletto, J. C. McCallum, and B. C. Johnson, "Infrared erbium photoluminescence enhancement in silicon carbide nanopillars," J. Appl. Phys. **130**, 145101 (2021).
[28]H. J. von Bardeleben, J. L. Cantin, A. Csóré, A. Gali, E. Rauls, and U. Gerstmann, "NV centers in 3*C*, 4*H*, and 6*H* silicon carbide: A variable platform for solid-state qubits and nanosensors," Phys. Rev. B **94**, 121202 (2016).
[29]T. Kimoto, "Material science and device physics in SiC technology for high-voltage power devices," Jpn. J. Appl. Phys. **54**, 040103 (2015).
[30]A. O. Evwaraye, S. R. Smith, and W. C. Mitchel, "Shallow levels in *n*-type 6H-silicon carbide as determined by admittance spectroscopy," J. Appl. Phys. **75**, 3472–3476 (1994).
[31]J. Bollmann and A. Venter, "Admittance spectroscopy or deep level transient spectroscopy: A contrasting juxtaposition," Physica B **535**, 237–241 (2018).
[32]L. Storasta, F. H. C. Carlsson, S. G. Sridhara, J. P. Bergman, A. Henry, T. Egilsson, A. Hallén, and E. Janzén, "Pseudodonor nature of the D_I defect in 4H-SiC," Appl. Phys. Lett. **78**, 46–48 (2001).
[33]R. Brunwin, B. Hamilton, P. Jordan, and A. Peaker, "Detection of minority-carrier traps using transient spectroscopy," Electron. Lett. **15**, 349 (1979).
[34]H. Nakane, M. Kato, Y. Ohkouchi, X. T. Trinh, I. G. Ivanov, T. Ohshima, and N. T. Son, "Deep levels related to the carbon antisite–vacancy pair in 4H-SiC," J. Appl. Phys. **130**, 065703 (2021).
[35]L. M. Porter and R. F. Davis, "A critical review of ohmic and rectifying contacts for silicon carbide," Mater. Sci. Eng., B **34**, 83 (1995).
[36]P. Pande, D. Haasmann, J. Han, H. A. Moghadam, P. Tanner, and S. Dimitrijev, "Electrical characterization of SiC MOS capacitors: A critical review," Microelectron. Reliab. **112**, 113790 (2020).
[37]L. M. Terman, "An investigation of surface states at a silicon/silicon oxide interface employing metal-oxide-silicon diodes," Solid-State Electron. **5**, 285–299 (1962).
[38]H. Yoshioka, T. Nakamura, and T. Kimoto, "Accurate evaluation of interface state density in SiC metal-oxide-semiconductor structures using surface potential based on depletion capacitance," J. Appl. Phys. **111**, 014502 (2012).
[39]W. A. Hill and C. C. Coleman, "A single-frequency approximation for interface-state density determination," Solid-State Electron. **23**, 987–993 (1980).
[40]C. N. Berglund, "Surface states at steam-grown silicon-silicon dioxide interfaces," IEEE Trans. Electron Devices **ED-13**, 701–705 (1966).
[41]R. Castagne and A. Vapaille, "Apparent interface state density introduced by the spatial fluctuations of surface potential in an MOS structure," Electron. Lett. **6**, 691–694 (1970).
[42]E. H. Nicollian and A. Goetzberger, "The Si-SiO interface–electrical properties as determined by the metal-insulator-silicon conductance technique," Bell Labs Tech. J. **46**, 1055–1133 (1967).
[43]H. Yoshioka, T. Nakamura, and T. Kimoto, "Characterization of very fast states in the vicinity of the conduction band edge at the SiO_2/SiC interface by low temperature conductance measurements," J. Appl. Phys. **115**, 014502 (2014).
[44]B. C. Johnson, J. Woerle, D. Haasmann, C. T. K. Lew, R. A. Parker, H. Knowles, B. Pingault, M. Atature, A. Gali, S. Dimitrijev, M. Camarda, and J. C. McCallum, "Optically active defects at the SiC/SiO_2 interface," Phys. Rev. Appl. **12**, 044024 (2019).
[45]D. Okamoto, H. Yano, Y. Oshiro, T. Hatayama, Y. Uraoka, and T. Fuyuki, "Investigation of near-interface traps generated by NO direct oxidation in C-face 4H-SiC metal–oxide–semiconductor structures," Appl. Phys. Express **2**, 021201 (2009).
[46]H. Yano, Y. Oshiro, D. Okamoto, T. Hatayama, and T. Fuyuki, "Instability of 4H-SiC MOSFET characteristics due to interface traps with long time constants," Mater. Sci. Forum **679-680**, 603–606 (2011).
[47]T. Aichinger, G. Rescher, and G. Pobegen, "Threshold voltage peculiarities and bias temperature instabilities of SiC MOSFETs," Microelectron. Reliab. **80**, 68–78 (2018).
[48]V. V. Afanasev, M. Bassler, G. Pensl, and M. Schulz, "Intrinsic SiC/SiO_2 interface states," Phys. Status Solidi A **162**, 321–337 (1997).
[49]V. V. Afanas'ev and A. Stesmans, "Interfacial defects in SiO_2 revealed by photon stimulated tunneling of electrons," Phys. Rev. Lett. **78**, 2437–2440 (1997).
[50]P. Deák, J. M. Knaup, T. Hornos, C. Thill, A. Gali, and T. Frauenheim, "The mechanism of defect creation and passivation at the SiC/SiO_2 interface," J. Phys. D: Appl. Phys. **40**, 6242–6253 (2007).
[51]C. Cochrane, P. M. Lenahan, and A. Lelis, "Identification of a silicon vacancy as an important defect in 4H SiC metal oxide semiconducting field effect transistor using spin dependent recombination," Appl. Phys. Lett. **100**, 023509 (2012).
[52]M. A. Anders, P. M. Lenahan, and A. J. Lelis, "Negative bias instability in 4H-SiC MOSFETs: Evidence for structural changes in the SiC," in *2015 IEEE International Reliability Physics Symposium* (IEEE, 2015), pp. 3E.4.1–3E.4.5.
[53]V. V. Afanas'ev, A. Stesmans, and C. I. Harris, "Observation of carbon clusters at the 4H-SiC/SiO_2 interface," Mater. Sci. Forum **264–268**, 857–860 (1997).
[54]K. C. Chang, N. T. Nuhfer, L. M. Porter, and Q. Wahab, "High-carbon concentrations at the silicon dioxide–silicon carbide interface identified by electron energy loss spectroscopy," Appl. Phys. Lett. **77**, 2186–2188 (2000).
[55]Y. Matsushita and A. Oshiyama, "A novel intrinsic interface state controlled by atomic stacking sequence at interfaces of SiC/SiO_2," Nano Lett. **17**, 6458–6463 (2017).
[56]J. Wong-Leung and B. G. Svensson, "Electric field assisted annealing and formation of prominent deep-level defect in ion-implanted *n*-type 4*H*-SiC," Appl. Phys. Lett. **92**, 142105 (2008).
[57]C. G. Hemmingsson, N. T. Son, A. Ellison, J. Zhang, and E. Janzén, "Negative-*U* centers in 4*H* silicon carbide," Phys. Rev. B **58**, R10119 (1998).
[58]B. Zippelius, J. Suda, and T. Kimoto, "High temperature annealing of n-type 4H-SiC: Impact on intrinsic defects and carrier lifetime," J. Appl. Phys. **111**, 033515 (2012).
[59]T. Hiyoshi and T. Kimoto, "Elimination of the major deep levels in n- and p-type 4H-SiC by two-step thermal treatment," Appl. Phys. Express **2**, 091101 (2009).
[60]L. S. Løvlie and B. G. Svensson, "Enhanced annealing of implantation-induced defects in 4H-SiC by thermal oxidation," Appl. Phys. Lett. **98**, 052108 (2011).
[61]L. S. Løvlie and B. G. Svensson, "Oxidation-enhanced annealing of implantation-induced $Z_{1/2}$ centers in 4H-SiC: Reaction kinetics and modeling," Phys. Rev. B **86**, 075205 (2012).
[62]T. Hiyoshi and T. Kimoto, "Reduction of deep levels and improvement of carrier lifetime in n-type 4H-SiC by thermal oxidation," Appl. Phys. Express **2**, 041101 (2009).
[63]S. Sasaki, K. Kawahara, G. Feng, G. Alfieri, and T. Kimoto, "Major deep levels with the same microstructures observed in n-type 4H-SiC and 6H-SiC," J. Appl. Phys. **109**, 013705 (2011).
[64]A. Koizumi, V. Markevich, N. Iwamoto, S. Sasaki, T. Ohshima, K. Kojima, T. Kimoto, K. Uchida, S. Nozaki, B. Hamilton, and A. R. Peaker, "E_1/E_2 traps in 6H-SiC studied with Laplace deep level transient spectroscopy," Appl. Phys. Lett. **102**, 032104 (2013).
[65]A. Salinaro, G. Pobegen, T. Aichinger, B. Zippelius, D. Peters, P. Friedrichs, and L. Frey, "Charge pumping measurements on differently passivated lateral 4H-SiC MOSFETs," IEEE Trans. Electron Devices **62**, 155–163 (2015).
[66]P. Habaš, Z. Prijić, and D. Pantić, "The application of charge-pumping technique to characterize the Si/SiO_2 interface in power VDMOSFETs," Microelectron. Eng. **28**, 171–174 (1995).

[67]X. Zhou, H. Su, R. Yue, G. Dai, J. Li, Y. Wang, and Z. Yu, "A deep insight into the degradation of 1.2-kV 4H-SiC MOSFETs under repetitive unclamped inductive switching stresses," IEEE Trans. Power Electron. **33**, 5251–5261 (2017).
[68]G. Groeseneken, H. E. Maes, N. Beltran, and R. F. De Keersmaecker, "A reliable approach to charge-pumping measurements in MOS transistors," IEEE Trans. Electron Devices **31**, 42–53 (1984).
[69]B. Djezzar, A. Smatti, and S. Oussalah, "Oxide-trap based on charge pumping (OTCP) extraction method for irradiated MOSFET devices: Part II (low frequencies)," in *2003 IEEE Nuclear Science Symposium. Conference Record (IEEE Cat. No. 03CH37515)* (IEEE, 2003), Vol. 1, pp. 601–605.
[70]D. Okamoto, H. Yano, T. Hatayama, Y. Uraoka, and T. Fuyuki, "Analysis of anomalous charge-pumping characteristics on 4H-SiC MOSFETs," IEEE Trans. Electron Devices **55**, 2013–2020 (2008).
[71]M. Tsuchiaki, H. Hara, T. Morimoto, and H. Iwai, "A new charge pumping method for determining the spatial distribution of hot-carrier-induced fixed charge in p-MOSFETs," IEEE Trans. Electron Devices **40**, 1768–1779 (1993).
[72]S. Mahapatra, C. D. Parikh, J. Vasi, V. Ramgopal Rao, and C. R. Viswanathan, "A direct charge pumping technique for spatial profiling of hot-carrier induced interface and oxide traps in MOSFETs," Solid-State Electron. **43**, 915–922 (1999).
[73]W. Chen, A. Balasinski, and T. Ma, "Lateral profiling of oxide charge and interface traps near MOSFET junctions," IEEE Trans. Electron Devices **40**, 187–196 (1993).
[74]N. Saks, G. Groeseneken, and I. DeWolf, "Characterization of individual interface traps with charge pumping," Appl. Phys. Lett. **68**, 1383–1385 (1996).
[75]J. W. Steeds, "Photoluminescence study of the carbon antisite-vacancy pair in 4*H*- and 6*H*-SiC," Phys. Rev. B **80**, 245202 (2009).
[76]E. Sörman, N. T. Son, W. M. Chen, O. Kordina, C. Hallin, and E. Janzén, "Silicon vacancy related defect in 4H and 6H SiC," Phys. Rev. B **61**, 2613–2620 (2000).
[77]W. F. Koehl, B. B. Buckley, F. J. Heremans, G. Calusine, and D. D. Awschalom, "Room temperature coherent control of defect spin qubits in silicon carbide," Nature **479**, 84–87 (2011).
[78]S. A. Zargaleh, B. Eble, S. Hameau, J.-L. Cantin, L. Legrand, M. Bernard, F. Margaillan, J.-S. Lauret, J.-F. Roch, H. J. von Bardeleben, E. Rauls, U. Gerstmann, and F. Treussart, "Evidence for near-infrared photoluminescence of nitrogen vacancy centers in 4*H*-SiC," Phys. Rev. B **94**, 060102 (2016).
[79]J. Steeds, G. Evans, L. Danks, S. Furkert, W. Voegeli, M. Ismail, and F. Carosella, "Transmission electron microscope radiation damage of 4H and 6H SiC studied by photoluminescence spectroscopy," Diamond Relat. Mater. **11**(12), 1923–1945 (2002).
[80]M. Rühl, C. Ott, S. Götzinger, M. Krieger, and H. Weber, "Controlled generation of intrinsic near-infrared color centers in 4H-SiC via proton irradiation and annealing," Appl. Phys. Lett. **113**, 122102 (2018).
[81]S. Castelletto, J. Maksimovic, T. Katkus, T. Ohshima, B. C. Johnson, and S. Juodkazis, "Color centers enabled by direct femto-second laser writing in wide bandgap semiconductors," Nanomaterials **11**, 72 (2021).
[82]A. Karim, I. Lyskov, S. P. Russo, and A. Peruzzo, "An *ab initio* effective solid-state photoluminescence by frequency constraint of cluster calculation," J. Appl. Phys. **128**, 233102 (2020).
[83]W. Carlos, E. Glaser, and B. Shanabrook, "Optical and magnetic resonance signatures of deep levels in semi-insulating 4H SiC," Physica B **340–342**, 151–155 (2003).
[84]W. E. Carlos, N. Y. Garces, E. R. Glaser, and M. A. Fanton, "Annealing of multivacancy defects in 4*H*-SiC," Phys. Rev. B **74**, 235201 (2006).
[85]J.-F. Wang, F.-F. Yan, Q. Li, Z.-H. Liu, H. Liu, G.-P. Guo, L.-P. Guo, X. Zhou, J.-M. Cui, J. Wang *et al.*, "Coherent control of nitrogen-vacancy center spins in silicon carbide at room temperature," Phys. Rev. Lett. **124**, 223601 (2020).
[86]G. Wolfowicz, C. P. Anderson, B. Diler, O. G. Poluektov, F. J. Heremans, and D. D. Awschalom, "Vanadium spin qubits as telecom quantum emitters in silicon carbide," Sci. Adv. **6**, eaaz1192 (2020).
[87]W. F. Koehl, B. Diler, S. J. Whiteley, A. Bourassa, N. T. Son, E. Janzén, and D. D. Awschalom, "Resonant optical spectroscopy and coherent control of Cr^{4+} spin ensembles in SiC and GaN," Phys. Rev. B **95**, 035207 (2017).
[88]B. Diler, S. J. Whiteley, C. P. Anderson, G. Wolfowicz, M. E. Wesson, E. S. Bielejec, F. Joseph Heremans, and D. D. Awschalom, "Coherent control and high-fidelity readout of chromium ions in commercial silicon carbide," npj Quantum Inf. **6**, 11 (2020).
[89]T. Bosma, G. J. J. Lof, C. M. Gilardoni, O. V. Zwier, F. Hendriks, B. Magnusson, A. Ellison, A. Gällström, I. G. Ivanov, N. T. Son, R. W. A. Havenith, and C. H. van der Wal, "Identification and tunable optical coherent control of transition-metal spins in silicon carbide," npj Quantum Inf. **4**, 48 (2018).
[90]J.-Y. Zhou, Q. Li, Z.-Y. Hao, F.-F. Yan, M. Yang, J.-F. Wang, W.-X. Lin, Z.-H. Liu, W. Liu, H. Li *et al.*, "Experimental determination of the dipole orientation of single color centers in silicon carbide," ACS Photonics **8**, 2384 (2021).
[91]P. G. Baranov, A. P. Bundakova, A. A. Soltamova, S. B. Orlinskii, I. V. Borovykh, R. Zondervan, R. Verberk, and J. Schmidt, "Silicon vacancy in SiC as a promising quantum system for single-defect and single-photon spectroscopy," Phys. Rev. B **83**, 125203 (2011).
[92]J. Davidsson, V. Ivády, R. Armiento, T. Ohshima, N. T. Son, A. Gali, and I. A. Abrikosov, "Identification of divacancy and silicon vacancy qubits in 6H-SiC," Appl. Phys. Lett. **114**, 112107 (2019).
[93]H. Itoh, M. Yoshikawa, I. Nashiyama, H. Okumura, S. Misawa, and S. Yoshida, "Photoluminescence of radiation induced defects in 3C-SiC epitaxially grown on si," J. Appl. Phys. **77**, 837–842 (1995).
[94]A. Lohrmann, S. Castelletto, J. Klein, T. Ohshima, M. Bosi, M. Negri, D. Lau, B. Gibson, S. Prawer, J. McCallum, and B. C. Johnson, "Activation and control of visible single defects in 4H-, 6H-, and 3C-SiC by oxidation," Appl. Phys. Lett. **108**, 021107 (2016).
[95]A. Lohrmann, N. Iwamoto, Z. Bodrog, S. Castelletto, T. Ohshima, T. Karle, A. Gali, S. Prawer, J. McCallum, and B. Johnson, "Single-photon emitting diode in silicon carbide," Nat. Commun. **6**, 1–7 (2015).
[96]A. Lohrmann, T. J. Karle, V. K. Sewani, A. Laucht, M. Bosi, M. Negri, S. Castelletto, S. Prawer, J. C. McCallum, and B. C. Johnson, "Integration of single-photon emitters into 3C-SiC microdisk resonators," ACS Photonics **4**, 462–468 (2017).
[97]S.-I. Sato, T. Honda, T. Makino, Y. Hijikata, S.-Y. Lee, and T. Ohshima, "Room temperature electrical control of single photon sources at 4H-SiC surface," ACS Photonics **5**, 3159–3165 (2018).
[98]J. Woerle, T. Prokscha, A. Hallén, and U. Grossner, "Interaction of low-energy muon with defect profiles in proton-irradiated Si and 4*H*-SiC," Phys. Rev. B **100**, 115202 (2019).
[99]C. T. K. Lew, N. Dontschuk, D. A. Broadway, J. P. Tetienne, J. C. McCallum, L. C. L. Hollenberg, and B. C. Johnson, "Investigation of charge carrier trapping in H-terminated diamond devices," Appl. Phys. Lett. **117**, 143507 (2020).
[100]A. L. Crook, C. P. Anderson, K. C. Miao, A. Bourassa, H. Lee, S. L. Bayliss, D. O. Bracher, X. Zhang, H. Abe, T. Ohshima, E. L. Hu, and D. D. Awschalom, "Purcell enhancement of a single silicon carbide color center with coherent spin control," Nano Lett. **20**, 3427–3434 (2020).
[101]S. C. Kitson, P. Jonsson, J. G. Rarity, and P. R. Tapster, "Intensity fluctuation spectroscopy of small numbers of dye molecules in a microcavity," Phys. Rev. A **58**, 620–627 (1998).
[102]C. K. Hong, Z. Y. Ou, and L. Mandel, "Measurement of subpicosecond time intervals between two photons by interference," Phys. Rev. Lett. **59**, 2044–2046 (1987).
[103]N. Morioka, C. Babin, R. Nagy, I. Gediz, E. Hesselmeier, D. Liu, M. Joliffe, M. Niethammer, D. Dasari, V. Vorobyov, R. Kolesov, R. Stöhr, J. Ul-Hassan, N. T. Son, T. Ohshima, P. Udvarhelyi, G. Thiering, A. Gali, J. Wrachtrup, and F. Kaiser, "Spin-controlled generation of indistinguishable and distinguishable photons from silicon vacancy centres in silicon carbide," Nat. Commun. **11**, 1–8 (2020).
[104]T. Umeda, Y. Ishitsuka, J. Isoya, N. T. Son, E. Janzén, N. Morishita, T. Ohshima, H. Itoh, and A. Gali, "EPR and theoretical studies of negatively charged carbon vacancy in 4*H*-SiC," Phys. Rev. B **71**, 193202 (2005).
[105]N. T. Son, P. Carlsson, J. ul Hassan, E. Janzén, T. Umeda, J. Isoya, A. Gali, M. Bockstedte, N. Morishita, T. Ohshima, and H. Itoh, "Divacancy in 4H-SiC," Phys. Rev. Lett. **96**, 055501 (2006).

[106]T. Umeda, N. T. Son, J. Isoya, E. Janzén, T. Ohshima, N. Morishita, H. Itoh, A. Gali, and M. Bockstedte, "Identification of the carbon antisite-vacancy pair in 4*H*-SiC," Phys. Rev. Lett. **96**, 145501 (2006).
[107]N. Mizuochi, S. Yamasaki, H. Takizawa, N. Morishita, T. Ohshima, H. Itoh, and J. Isoya, "EPR studies of the isolated negatively charged silicon vacancies in *n*-type 4*H* and 6*H*-SiC: Identification of C_{3v} symmetry and silicon sites," Phys. Rev. B **68**, 165206 (2003).
[108]G. R. Eaton, S. S. Eaton, D. P. Barr, and R. T. Weber, *Quantitative EPR* (Springer Science & Business Media, 2010).
[109]D. Kaplan, I. Solomon, and N. Mott, "Explanation of the large spin-dependent recombination effect in semiconductors," J. Phys. Lett. **39**, 51 (1978).
[110]G. Gruber, J. Cottom, R. Meszaros, M. Koch, G. Pobegen, T. Aichinger, D. Peters, and P. Hadley, "Electrically detected magnetic resonance of carbon dangling bonds at the Si-face 4H-SiC/SiO_2 interface," J. Appl. Phys. **123**, 161514 (2018).
[111]T. Aichinger and P. M. Lenahan, "Giant amplification of spin dependent recombination at heterojunctions through a gate controlled bipolar effect," Appl. Phys. Lett. **101**, 083504 (2012).
[112]B. C. Bittel, P. M. Lenahan, J. T. Ryan, J. Fronheiser, and A. J. Lelis, "Spin dependent charge pumping in SiC metal-oxide-semiconductor field-effect-transistors," Appl. Phys. Lett. **99**, 083504 (2011).
[113]M. Anders, P. Lenahan, and A. Lelis, "Multi-resonance frequency spin dependent charge pumping and spin dependent recombination-applied to the 4H-SiC/SiO_2 interface," J. Appl. Phys. **122**, 234503 (2017).
[114]J. Cottom, G. Gruber, G. Pobegen, T. Aichinger, and A. L. Shluger, "Recombination defects at the 4H-SiC/SiO_2 interface investigated with electrically detected magnetic resonance and *ab initio* calculations," J. Appl. Phys. **124**, 045302 (2018).
[115]T. Umeda, T. Kobayashi, M. Sometani, H. Yano, Y. Matsushita, and S. Harada, "Carbon dangling-bond center (carbon P_b center) at 4H-SiC (0001)/SiO_2 interface," Appl. Phys. Lett. **116**, 071604 (2020).
[116]T. Umeda, Y. Nakano, E. Higa, T. Okuda, T. Kimoto, T. Hosoi, H. Watanabe, M. Sometani, and S. Harada, "Electron-spin-resonance and electrically detected-magnetic-resonance characterization on P_{bC} center in various 4H-SiC (0001)/SiO_2 interfaces," J. Appl. Phys. **127**, 145301 (2020).
[117]C. J. Cochrane, J. Blacksberg, M. A. Anders, and P. M. Lenahan, "Vectorized magnetometer for space applications using electrical readout of atomic scale defects in silicon carbide," Sci. Rep. **6**, 37077 (2016).
[118]D. Simin, V. A. Soltamov, A. V. Poshakinskiy, A. N. Anisimov, R. A. Babunts, D. O. Tolmachev, E. N. Mokhov, M. Trupke, S. A. Tarasenko, A. Sperlich, P. G. Baranov, V. Dyakonov, and G. V. Astakhov, "All-optical dc nanotesla magnetometry using silicon vacancy fine structure in isotopically purified silicon carbide," Phys. Rev. X **6**, 031014 (2016).
[119]M. Widmann, S. Y. Lee, T. Rendler, N. T. Son, H. Fedder, S. Paik, L. P. Yang, N. Zhao, S. Yang, I. Booker, A. Denisenko, M. Jamali, S. Ali Momenzadeh, I. Gerhardt, T. Ohshima, A. Gali, E. Janzén, and J. Wrachtrup, "Coherent control of single spins in silicon carbide at room temperature," Nat. Mater. **14**, 164–168 (2015).
[120]M. Atatüre, D. Englund, N. Vamivakas, S.-Y. Lee, and J. Wrachtrup, "Material platforms for spin-based photonic quantum technologies," Nat. Rev. Mater. **3**, 38–51 (2018).
[121]D. J. Christle, A. L. Falk, P. Andrich, P. V. Klimov, J. U. Hassan, N. T. Son, E. Janzén, T. Ohshima, and D. D. Awschalom, "Isolated electron spins in silicon carbide with millisecond coherence times," Nat. Mater. **14**, 160–163 (2015).
[122]D. Simin, F. Fuchs, H. Kraus, A. Sperlich, P. G. Baranov, G. V. Astakhov, and V. Dyakonov, "High-precision angle-resolved magnetometry with uniaxial quantum centers in silicon carbide," Phys. Rev. Appl. **4**, 014009 (2015).
[123]M. Niethammer, M. Widmann, S.-Y. Lee, P. Stenberg, O. Kordina, T. Ohshima, N. T. Son, E. Janzén, and J. Wrachtrup, "Vector magnetometry using silicon vacancies in 4*H*-SiC under ambient conditions," Phys. Rev. Appl. **6**, 034001 (2016).
[124]M. Widmann, M. Niethammer, D. Y. Fedyanin, I. A. Khramtsov, T. Rendler, I. D. Booker, J. Ul Hassan, N. Morioka, Y.-C. Chen, I. G. Ivanov, N. T. Son, T. Ohshima, M. Bockstedte, A. Gali, C. Bonato, S.-Y. Lee, and J. Wrachtrup, "Electrical charge state manipulation of single silicon vacancies in a silicon carbide quantum optoelectronic device," Nano Lett. **19**, 7173–7180 (2019).
[125]F. Fuchs, B. Stender, M. Trupke, D. Simin, J. Pflaum, V. Dyakonov, and G. V. Astakhov, "Engineering near-infrared single-photon emitters with optically active spins in ultrapure silicon carbide," Nat. Commun. **6**, 1–7 (2015).
[126]H. B. Banks, Ö. O. Soykal, R. L. Myers-Ward, D. K. Gaskill, T. L. Reinecke, and S. G. Carter, "Resonant optical spin initialization and readout of single silicon vacancies in 4*H*-SiC," Phys. Rev. Appl. **11**, 1 (2019).
[127]R. Nagy, M. Niethammer, M. Widmann, Y. C. Chen, P. Udvarhelyi, C. Bonato, J. U. Hassan, R. Karhu, I. G. Ivanov, N. T. Son, J. R. Maze, T. Ohshima, Ö. O. Soykal, Á. Gali, S. Y. Lee, F. Kaiser, and J. Wrachtrup, "High-fidelity spin and optical control of single silicon-vacancy centres in silicon carbide," Nat. Commun. **10**, 1954 (2019).
[128]D. Simin, H. Kraus, A. Sperlich, T. Ohshima, G. V. Astakhov, and V. Dyakonov, "Locking of electron spin coherence above 20 ms in natural silicon carbide," Phys. Rev. B **95**, 161201 (2017).
[129]M. Niethammer, M. Widmann, T. Rendler, N. Morioka, Y.-C. Chen, R. Stöhr, J. U. Hassan, S. Onoda, T. Ohshima, S.-Y. Lee *et al.*, "Coherent electrical readout of defect spins in silicon carbide by photo-ionization at ambient conditions," Nat. Commun. **10**, 1–8 (2019).
[130]C. P. Anderson, E. O. Glen, C. Zeledon, A. Bourassa, Y. Jin, Y. Zhu, C. Vorwerk, A. L. Crook, H. Abe, J. Ul-Hassan *et al.*, "Five-second coherence of a single spin with single-shot readout in silicon carbide," arXiv:2110.01590 (2021).
[131]G. Kramberger, V. Cindro, I. Mandić, M. Mikuž, M. Milovanović, M. Zavrtanik, and K. V. Žagar, "Investigation of irradiated silicon detectors by edge-TCT," IEEE Trans. Nucl. Sci. **57**, 2294–2302 (2010).
[132]C. Dorfer, D. Hits, L. Kasmi, G. Kramberger, M. Lucchini, M. Mikuž, and R. Wallny, "Three-dimensional charge transport mapping by two-photon absorption edge transient-current technique in synthetic single-crystalline diamond," Appl. Phys. Lett. **114**, 203504 (2019).
[133]A. Gorišek, V. Cindro, G. Kramberger, I. Mandić, M. Mikuž, M. Muškinja, and M. Zavrtanik, "The edge transient-current technique (E-TCT) with high energy hadron beam," Nucl. Instrum. Methods Phys. Res., Sect. A **831**, 250–253 (2016).
[134]B. D. Patterson, "Muonium states in semiconductors," Rev. Mod. Phys. **60**, 69–159 (1988).
[135]S. F. J. Cox, "Implanted muon studies in condensed matter science," J. Phys. C: Solid State Phys. **20**, 3187–3319 (1987).
[136]R. F. Kiefl and T. L. Estle, "Muonium in semiconductors," in *Semiconductors and Semimetals*, edited by J. I. Pankove and N. M. Johnson (Elsevier, 1991), Vol. 34, Chap. 15, pp. 547–584.
[137]E. Westhauser, E. Albert, M. Hamma, E. Recknagel, A. Weidinger, and P. Moser, "Mu TO Mu^* transition in electron irradiated silicon," Hyperfine Interact. **32**, 589–593 (1986).
[138]V. A. Gordeev, R. F. Konopleva, V. G. Firsov, Y. V. Obukhov, Y. V. Gorelkinskii, and N. N. Nevinnyi, "Equivalent states of muonium and implanted hydrogen in silicon (experiment)," Hyperfine Interact. **60**, 717–722 (1990).
[139]J. Woerle, M. E. Bathen, T. Prokscha, A. Galeckas, H. M. Ayedh, L. Vines, and U. Grossner, "Muon interaction with negative-U and high-spin-State defects: Differentiating between C and Si vacancies in 4*H*-SiC," Phys. Rev. Appl. **14**, 054053 (2020).
[140]J. Woerle, T. Prokscha, and U. Grossner, "Low-energy muons as a tool for a depth-resolved analysis of the SiO_2/4H-SiC interface," Mater. Sci. Forum **1004**, 581–586 (2020).
[141]J. P. Perdew, K. Burke, and M. Ernzerhof, "Generalized gradient approximation made simple," Phys. Rev. Lett. **77**, 3865–3868 (1996).
[142]J. Heyd, G. E. Scuseria, and M. Ernzerhof, "Hybrid functionals based on a screened Coulomb potential," J. Chem. Phys. **118**, 8207–8215 (2003).
[143]C. Freysoldt, B. Grabowski, T. Hickel, J. Neugebauer, G. Kresse, A. Janotti, and C. G. Van de Walle, "First-principles calculations for point defects in solids," Rev. Mod. Phys. **86**, 253–305 (2014).

[144]S. B. Zhang and J. E. Northrup, "Chemical potential dependence of defect formation energies in GaAs: Application to Ga self-diffusion," Phys. Rev. Lett. **67**, 2339 (1991).
[145]C. G. Van de Walle, D. B. Laks, G. F. Neumark, and S. T. Pantelides, "First-principles calculations of solubilities and doping limits: Li, Na, and N in ZnSe," Phys. Rev. B **47**, 9425–9434 (1993).
[146]M. E. Bathen, A. Galeckas, J. Müting, H. M. Ayedh, U. Grossner, J. Coutinho, Y. K. Frodason, and L. Vines, "Electrical charge state identification and control for the silicon vacancy in 4H-SiC," npj Quantum Inf. **5**, 111 (2019).
[147]R. Karsthof, M. E. Bathen, A. Galeckas, and L. Vines, "Conversion pathways of primary defects by annealing in proton-irradiated *n*-type 4*H*-SiC," Phys. Rev. B **102**, 184111 (2020).
[148]J. Coutinho, J. D. Gouveia, T. Makino, T. Ohshima, I. C. V. Pastuović, L. Bakrač, T. Brodar, and I. Capan, "*M* center in 4*H*-SiC is a carbon self-interstitial," Phys. Rev. B **103**, L180102 (2021).
[149]H. Jónnson, G. Mills, and K. W. Jacobsen, "Nudged elastic band method for finding minimum energy paths of transitions," in *Classical and Quantum Dynamics in Condensed Phase Simulations* (World Scientific, 1998), pp. 385–404.
[150]Z. Zolnai, N. T. Son, C. Hallin, and E. Janzén, "Annealing behavior of the carbon vacancy in electron-irradiated 4*H*-SiC," J. Appl. Phys. **96**, 2406–2408 (2004).
[151]M. Bockstedte, A. Mattausch, and O. Pankratov, "*Ab initio* study of the migration of intrinsic defects in 3*C*-SiC," Phys. Rev. B **68**, 205201 (2003).
[152]M. E. Bathen, J. Coutinho, H. M. Ayedh, J. U. Hassan, I. Farkas, S. Öberg, Y. K. Frodason, B. G. Svensson, and L. Vines, "Anisotropic and plane-selective migration of the carbon vacancy in SiC: Theory and experiment," Phys. Rev. B **100**, 014103 (2019).
[153]R. Kuate Defo, X. Zhang, D. Bracher, G. Kim, E. Hu, and E. Kaxiras, "Energetics and kinetics of vacancy defects in 4*H*-SiC," Phys. Rev. B **98**, 104103 (2018).
[154]K. Szász, V. Ivády, I. A. Abrikosov, E. Janzén, M. Bockstedte, and A. Gali, "Spin and photophysics of carbon-antisite vacancy defect in 4*H* silicon carbide: A potential quantum bit," Phys. Rev. B **91**, 121201 (2015).
[155]J. Coutinho, "Theory of the thermal stability of silicon vacancies and interstitials in 4H-SiC," Crystals **11**, 167 (2021).
[156]C. E. Dreyer, A. Alkauskas, J. L. Lyons, A. Janotti, and C. G. Van de Walle, "First-principles calculations of point defects for quantum technologies," Annu. Rev. Mater. Res. **48**, 1–26 (2018).
[157]A. Gali, "Excitation properties of silicon vacancy in silicon carbide," Mater. Sci. Forum **717–720**, 255–258 (2012).
[158]A. Gali, E. Janzén, P. Deák, G. Kresse, and E. Kaxiras, "Theory of spin-conserving excitation of the *N-V-* center in diamond," Phys. Rev. Lett. **103**, 186404 (2009).
[159]V. Ivády, J. Davidsson, N. T. Son, T. Ohshima, I. A. Abrikosov, and A. Gali, "Identification of Si-vacancy related room-temperature qubits in 4*H* silicon carbide," Phys. Rev. B **96**, 161114(R) (2017).
[160]A. Alkauskas, B. B. Buckley, D. D. Awschalom, and C. G. Van de Walle, "First-principles theory of the luminescence lineshape for the triplet transition in diamond NV centres," New J. Phys. **16**, 073026 (2014).
[161]A. Hashemi, C. Linderälv, A. V. Krasheninnikov, T. Ala-Nissila, P. Erhart, and H.-P. Komsa, "Photoluminescence line shapes for color centers in silicon carbide from density functional theory calculations," Phys. Rev. B **103**, 125203 (2021).
[162]Z. Shang, A. Hashemi, Y. Berencen, H.-P. Komsa, P. Erhart, S. Zhou, M. Helm, A. V. Krasheninnikov, and G. V. Astakhov, "Local vibrational modes of Si vacancy spin qubits in SiC," Phys. Rev. B **101**, 144109 (2020).
[163]P. Udvarhelyi, G. Thiering, N. Morioka, C. Babin, F. Kaiser, D. Lukin, T. Ohshima, J. Ul-Hassan, N. T. Son, J. Vucković, J. Wrachtrup, and A. Gali, "Vibronic states and their effect on the temperature and strain dependence of silicon-vacancy qubits in 4*H*-SiC," Phys. Rev. Appl. **13**, 054017 (2020).
[164]M. E. Bathen, L. Vines, and J. Coutinho, "First-principles calculations of stark shifts of electronic transitions for defects in semiconductors: The Si vacancy in 4*H*-SiC," J. Phys.: Condens. Matter. **33**, 075502 (2020).
[165]D. J. McCrory, M. A. Anders, J. T. Ryan, P. R. Shrestha, K. P. Cheung, P. M. Lenahan, and J. P. Campbell, "Wafer-level electrically detected magnetic resonance: Magnetic resonance in a probing station," IEEE Trans. Device Mater. Reliab. **18**, 139–143 (2018).
[166]N. Mizuochi, S. Yamasaki, H. Takizawa, N. Morishita, T. Ohshima, H. Itoh, and J. Isoya, "Continuous-wave and pulsed EPR study of the negatively charged silicon vacancy with $s = 3/2$ and C_{3v} symmetry in *n*-type 4*H*-SiC," Phys. Rev. B **66**, 235202 (2002).
[167]I. Capan, T. Brodar, Ž. Pastuović, R. Siegele, T. Ohshima, S.-I. Sato, T. Makino, L. Snoj, V. Radulović, J. Coutinho, V. J. B. Torres, and K. Demmouche, "Double negatively charged carbon vacancy at the h- and k-sites in 4H-SiC: Combined laplace-DLTS and DFT study," J. Appl. Phys. **123**, 161597 (2018).
[168]H. M. Ayedh, A. Hallén, and B. G. Svensson, "Elimination of carbon vacancies in 4H-SiC epi-layers by near-surface ion implantation: Influence of the ion species," J. Appl. Phys. **118**, 175701 (2015).
[169]H. M. Ayedh, R. Nipoti, A. Hallén, and B. G. Svensson, "Elimination of carbon vacancies in 4H-SiC employing thermodynamic equilibrium conditions at moderate temperatures," Appl. Phys. Lett. **107**, 252102 (2015).
[170]M. T. Madzik, S. Asaad, A. Youssry, B. Joecker, K. M. Rudinger, E. Nielsen, K. C. Young, T. J. Proctor, A. D. Baczewski, A. Laucht, V. Schmitt, F. E. Hudson, K. M. Itoh, A. M. Jakob, B. C. Johnson, D. N. Jamieson, A. S. Dzurak, C. Ferrie, R. Blume-Kohout, and A. Morello, "Precision tomography of a three-qubit donor quantum processor in silicon," Nature **601**, 348–353 (2022).